(2)

DTIC FILE COPY

AD-A218 417

SECURITY CLASSIFICATION OF THIS PAGE

REPORT DOCUMENTATION PAGE

Form Approved OMB No 0704-0188

DTIC ELECTE FEB 27 1990 S D

1a. REPORT SECURITY CLASSIFICATION: Unclassified	1b. RESTRICTIVE MARKINGS
2a. SECURITY CLASSIFICATION AUTHORITY	3. DISTRIBUTION/AVAILABILITY OF REPORT: unlimited
2b. DECLASSIFICATION/DOWNGRADING SCHEDULE	
4. PERFORMING ORGANIZATION REPORT NUMBER(S): NO	5. MONITORING ORGANIZATION REPORT NUMBER(S): AFOSR-TR- 90-0205
6a. NAME OF PERFORMING ORGANIZATION: Univerefty of Rochester; 6b. OFFICE SYMBOL (If applicable): LLE	7a. NAME OF MONITORING ORGANIZATION: Air Force Office of Scientific Research
6c. ADDRESS (City, State, and ZIP Code): Laboratory for Laser Energetics, 250 E. River Road, Rochester, NY 14623-1299	7b. ADDRESS (City, State, and ZIP Code): AFOSR/NE, Bldg. 410, Bolling Air Force Base, DC 20332-6448
8a. NAME OF FUNDING/SPONSORING ORGANIZATION: A.F. Ofc. of Scientific Research; 8b. OFFICE SYMBOL (If applicable): [redacted]NE	9. PROCUREMENT INSTRUMENT IDENTIFICATION NUMBER: AFOSR-87-0327
8c. ADDRESS (City, State, and ZIP Code): AFOSR/[redacted], Bldg. 410, Bolling Air Force Base, DC 20332-6448	10. SOURCE OF FUNDING NUMBERS: PROGRAM ELEMENT NO. 61102F; PROJECT NO. 2306; TASK NO. B1; WORK UNIT ACCESSION NO.

11. TITLE (Include Security Classification)
TIME-RESOLVED SURFACE STRUCTURAL STUDY BY PICOSECOND REFLECTION HIGH-ENERGY ELECTRON DIFFRACTION

12. PERSONAL AUTHOR(S)
Elsayed-Ali, Hani E.

13a. TYPE OF REPORT	13b. TIME COVERED	14. DATE OF REPORT (Year, Month, Day)	15. PAGE COUNT
Final Report	FROM 87/8/1 TO 89/1/31	89/3/21	53

16. SUPPLEMENTARY NOTATION

17. COSATI CODES: FIELD	GROUP	SUB-GROUP	18. SUBJECT TERMS (Continue on reverse if necessary and identify by block number)

19. ABSTRACT (Continue on reverse if necessary and identify by block number)

The objective of this program was to develop an instrument for characterization of nanosecond and picosecond time evolution of surface properties. This instrument was developed based on the technique of picosecond time-resolved reflection high-energy electron diffraction (RHEED).

The basic idea of this technique is the utilization of 150 ps laser pulses to generate electron pulses by the photoelectric effect. The photogenerated electrons are accelerated, focussed, and collimated using electron optics. Only a very small fraction of the laser pulse energy is needed to generate the fast (10-30 kV) well-collimated electron pulses; thus, most of the laser energy is available for sample irradiation. The synchronization between the laser pulse irradiating the sample and the electron pulse probing the surface is within a few picoseconds. Thus, by time delaying the electron pulse relative to the laser pulse, it is possible to probe the surface structure of the studied crystal after

(continued on reverse) (see stach)

20. DISTRIBUTION/AVAILABILITY OF ABSTRACT	21. ABSTRACT SECURITY CLASSIFICATION
☒ UNCLASSIFIED/UNLIMITED ☐ SAME AS RPT. ☐ DTIC USERS	Unclassified
22a. NAME OF RESPONSIBLE INDIVIDUAL: Maj Gernot Pomrenke	22b. TELEPHONE (Include Area Code): (202)767-4931
	22c. OFFICE SYMBOL: NE

DD Form 1473, JUN 86 Previous editions are obsolete. SECURITY CLASSIFICATION OF THIS PAGE

90 02 23 064

FINAL REPORT ON

GRANT NO. AFOSR-87-0327

"TIME-RESOLVED SURFACE STRUCTURAL STUDY BY PICOSECOND REFLECTION HIGH-ENERGY ELECTRON DIFFRACTION"

Prepared for

UNITED STATES AIR FORCE
AIR FORCE OFFICE OF SCIENTIFIC RESEARCH (AFSC)
BOLLING AIR FORCE BASE, DC 20332-6448

for the period

1 August 1987 to 31 January 1989

Submitted by

Hani E. Elsayed-Ali
Principal Investigator

LABORATORY FOR LASER ENERGETICS
University of Rochester
250 East River Road
Rochester, New York 14623-1299

TIME-RESOLVED SURFACE STRUCTURAL STUDY BY PICOSECOND REFLECTION HIGH-ENERGY ELECTRON DIFFRACTION

Dr Hani Elsayed-Ali (716) 275-5101
University of Rochester
Ultrfast Science & Technology
Rochester NY 14623-1299

Technical Abstract:

OBJECTIVE - The goal of this work is to develop an instrument for characterizing the nano- and picosecond time evolution of surface properties. APPROACH - The techniques of ultrafast laser spectroscopy will be applied to the development of a subpicosecond, reflection, high-energy electron diffraction apparatus. A subpicosecond laser pulse will be split in a beam splitter. The first pulse will interact in some fashion with a well-characterized semiconductor or metal surface in an ultrahigh vacuum. Meanwhile, the second pulse will illuminate a thin metal foil that serves as a photocathode electron source, also in the vacuum chamber. By careful construction of the electron optics, a well-collimated burst of electrons will interact with the surface after the arrival of the original pulse. Imaging this reflected electron burst on a fluorescent screen or on a multichannel analyzer provides information on the state of the surface structure as a function of the time lapse since the arrival of the first laser pulse.

87NE101
Capt Kevin Malloy
2305/A9

TABLE OF CONTENTS

ABSTRACT

The objective of this program was to develop an instrument for characterization of nanosecond and picosecond time evolution of surface properties. This instrument was developed based on the technique of picosecond time-resolved reflection high-energy electron diffraction (RHEED).

The basic idea of this technique is the utilization of ~150 ps laser pulses to generate electron pulses by the photoelectric effect. These electron pulses are both a temporal and a spatial replica of the deriving laser pulses. The photogenerated electrons are accelerated, focussed, and collimated using electron optics. Only a very small fraction of the laser pulse energy is needed to generate the fast (10–30 kV) well-collimated electron pulses; thus, most of the laser energy is available for sample irradiation. The synchronization between the laser pulse irradiating the sample and the electron pulse probing the surface is within a few picoseconds. Thus, by time delaying the electron pulse relative to the laser pulse, it is possible to probe the surface structure of the studied crystal after laser irradiation with up to ~100 ps time resolution. This is done by spatially delaying the part of the laser pulse that is used to irradiate the sample.

An ultrahigh vacuum facility containing a picosecond RHEED capability was developed and tested. Details of this facility are described. This system was utilized to study surface heating and cooling of a Pb(110) crystal. In addition to providing a structural probe, quantitative analysis of picosecond RHEED patterns provides a direct time-resolved lattice temperature probe. Pattern sensitivity to temperature is due to the surface Debye-Waller factor which results in a reduction of the intensity of the elastically scattered electrons with lattice heating. The development of a picosecond time-resolved surface temperature probe (thermometer) is of a great value to the understanding of the kinetics of many relevant surface reactions (e.g., pulsed laser assisted metal deposition in

microelectronics fabrication, surface reconstruction, surface melting, other diffusion induced and diffusionless surface reactions, desorption, and surface chemical reactions.

Results on surface melting of the Pb(110) crystal are presented. The existence of a surface melting transformation at temperatures below the bulk melting point was demonstrated in our experiments. Time-resolved observation of the cooling of Pb(110) after fast heating with a laser pulse are also presented.

I. INTRODUCTION

The use of ultrafast lasers (nanosecond and picosecond) to induce and probe chemical and physical processes at surfaces is a subject of a great deal of interest.[1] In particular, laser processing of electronic materials with the goal of annealing damage due to ion bombardment, formation of a new metastable phases by fast quenching, and deposition of thin films pyroletically or photolytically are under intensive studies in many laboratories. In addition to their uses in device fabrication, ultrafast lasers are also being used to probe surface chemical and physical reactions relevant to the fabrication of electronic materials. The fast heating rates that such lasers provide cannot be attained by other means. This offers the capability of probing and, to a large extent, controlling the relative yields of products from competing surface chemical reactions. Many surface phase transformations relevant to the fabrication of electronic devices occur at exceedingly fast time scales ($>10^{-9}$ seconds) that ultrafast laser technology provide the only means to time-resolve the growth and perhaps the nucleation stages of such transformations. For example, surface reconstruction of Si and GaAs is known to alter the physical and chemical properties of the first few atomic monolayers of these materials. It is well established that depending on the surface structure, the sticking coefficient can be significantly altered. An understanding of such surface phase transformations could have wide implications in better controlling the fabrication of electronic devices by chemical vapor deposition and molecular beam epitaxy.

Time-resolved observations of phenomena accompanying pulsed laser irradiation have been accomplished by several different techniques. These include optical probing (both reflection and transmissions),[2–6] photoconductivity measurement,[7] x-ray diffraction,[8] Raman scattering,[9] and time-of-flight mass spectrometry.[10] None of these techniques provides a surface structural and temperature probe that can be limited to the first few monolayers. Although second-harmonic generation could provide a surface structural and temperature probe[11], the structural information it offers is indirect and somewhat ambiguous.[12] Second-harmonic generation can be sensitive to surface temperature due to electron-band structural changes. This, however, is viable only when resonantly enhanced by the second harmonic being near the interband transition.[13] This limits the applicability of this technique to a few materials.

The evolution of surface temperature after pulsed laser irradiation is typically obtained by a solution of the heat diffusion equation rather than any experimental measurement. Although such models seem to provide reasonable accuracy in a few simple cases where the material properties are well measured, many other cases, particularly those involving chemical surface reactions, cannot be simulated by these models with any accuracy.

Indeed, knowledge of the structure and temperature of these initial atomic layers that is of prime importance to the understanding and possibly controlling thin film fabrication processes. This requires the development of a direct time-resolved surface structural and temperature probe capable of monitoring the complex processes of surface phase transitions and reactions. The objective of this program was to develop an instrument for nanosecond and picosecond time-resolved monitoring of surface structure and temperature based on reflection high energy electron diffraction (RHEED).

Electron diffraction (both high-energy and low-energy) provides a "natural" surface probe that is well-developed and has been utilized for many decades in surface studies.[14-21]. However, the development of such a technique with picosecond time

resolution required the solution of several challenging technological problems. These included the production of picosecond "monoenergetic" electron burst to be used for electron diffraction, synchronization of such an electron burst with a laser heating pulse, and development of techniques to monitor the picosecond electron diffraction pattern. These tasks were accomplished by our development of an ultrahigh vacuum picosecond RHEED facility. Details of this system will be described along with its utilization to study surface heating and melting of Pb(110) crystal.

The basic idea of this technique is the utilization of a picosecond laser pulse to create an electron pulse with equal time duration. These photogenerated electrons can be collimated and focussed to make them suitable to obtain a good RHEED pattern from the surface of the studied crystal. A schematic diagram of this technique is shown in Fig. 1. Typically we use a Nd:YAG laser ($\lambda = 1.06\ \mu m$) to irradiate the sample while the electron probing pulse is generated by irradiation of a photocathode with a frequency quadrupled Nd:YAG ($\lambda = 0.266\ \mu m$). Frequency quadrupling allows us to use a rugged metallic photocathode. Only a very small part of the Nd:YAG fundamental is converted to the ultraviolet, thus, most of the laser energy is available to irradiate the sample. By spatially delaying the ultraviolet laser pulse from the fundamental it is possible to obtain RHEED patterns of the studied sample from a few hundred picoseconds to up to tens of nanoseconds after laser irradiation.

II. WHY HIGH-ENERGY ELECTRON DIFFRACTION

The main reason why we chose to initially develop the picosecond reflection high energy electron diffraction (versus low energy) is the limitations imposed on the number of electrons per pulse for such fast regimes due to space charge effects. Since the electron energy in RHEED systems is typically 10–50 kV (versus 50–500 eV in LEED), space charge limitations on the number of electrons per pulse are significantly less in RHEED. Indeed, we obtained good RHEED patterns using a single ~100 ps electron pulse.[22]

- picosecond RHEED (surface phase transitions)

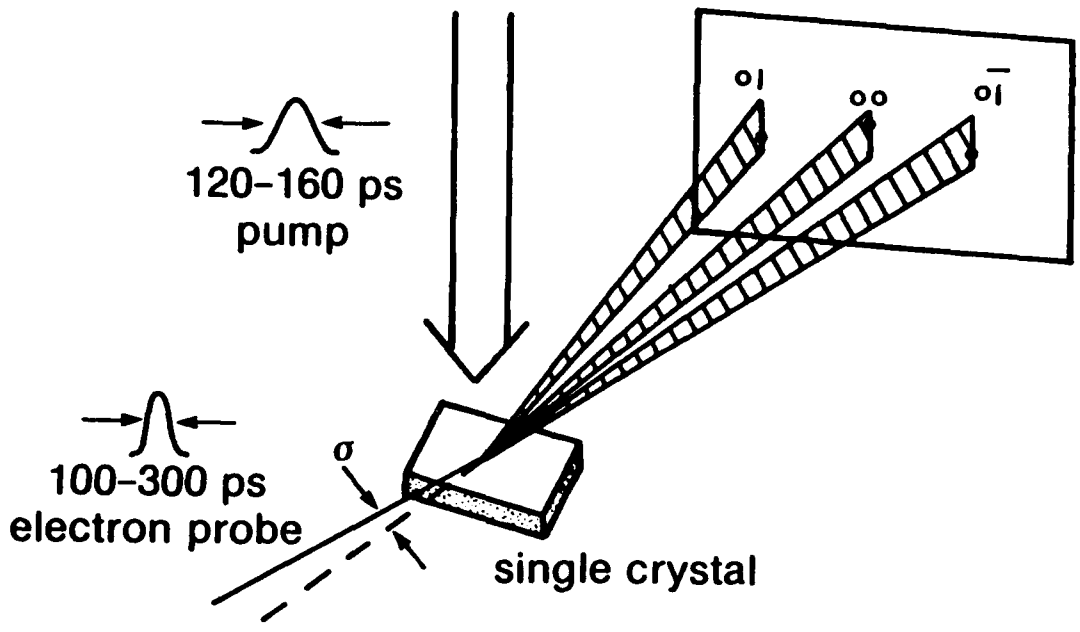

Z239

Fig. 1 Picosecond reflection high-energy electron diffraction (RHEED). The electron pulse generating the RHEED pattern is well synchronized with the pump laser pulse.

Other considerations, in addition to space charge limitations, include the following:[14,21]

1. The atomic scattering factors for RHEED are compatible to that for LEED. Thus, both cases have compatible limitations on their resolution.
2. The scattering factors in RHEED are dependent on sin (ϑ) where ϑ is the angle of incidence. Thus, by simply varying this angle of incidence (rather than changing electron energy), it is possible to change the thickness of the probed surface layer in the range of 1–20 Å.
3. Due to difficulties associated with low-energy electron diffraction (e.g., inelastic scattering and the effect of atomic charge), high-energy electron diffraction results tend to be easier to interpret.
4. The observation of the diffraction pattern in RHEED, in general, is simpler than for LEED since no electron energy amplifying stage is needed and since the pattern can be recorded normal to the electron beam (versus a large angular region for LEED).

A difficulty associated in RHEED systems is the need for multiazimuthal measurements (at least two) to allow full characterization of the surface. This is due to the fact that the RHEED pattern represents only one section of the reciprocal lattice normal to the surface.

Quantitative analysis of RHEED patterns can provide significant information on surface structure and topography. Typically, RHEED patterns consist of:

- Surface diffraction rods due to the relaxation of the third Laue condition for grazing incidence.
- Kikuchi bands and lines due to the inelastically scattered electrons.
- Diffraction spots due to microscopic undulation of the surface or the formation of aspirates (surface roughness).

The existence and the relative location of the diffraction rods (streaks) provide the information on surface order. The length of these RHEED streaks, with a characteristic

angle of incidence, provides information on surface steps.[20,23] Surface facets can be detected by additional streaks which are not normal to the shadow edge.[24] Surface aspirates and undulation can be detected by the existence of diffraction spots superimposed on the streaks.[20] The existence of the Kikuchi bands and lines is an indication of crystal perfection.[14] During surface melting, these bands and lines can still be seen since they originate from relatively deeper layers than the surface layers which give the diffraction rods.[25] The wealth of information on the surface properties which is possible to obtain from the RHEED patterns makes picosecond RHEED a powerful tool to study the dynamics of fast surface phase transformations, as in the case of surface melting.

III. VACUUM CHAMBER

A schematic diagram of the all stainless steel ultrahigh vacuum chamber is shown in Fig. 2. The chamber is pumped by two independent pumping stations. The first consists of a 300 l/s differential ion pump and a titanium sublimation pump. These are surrounded with a cryogenic panel and are isolated from the chamber with a poppet valve. System roughing is accomplished by two sorption pumps isolated from the chamber by an ultrahigh vacuum valve. Using this pumping system, the base pressure in the chamber is in the 10^{-10} Torr after a bakeout. The second pumping system consists of a 300 l/s turbomolecular pump supported by a two-stage mechanical forepump. This system is isolated from the chamber by a pneumatic 6-inch ultrahigh vacuum swing valve. A base pressure in the high 10^{-10} Torr can also be achieved using this pumping system after a bakeout.

The combination of two pumping systems based on a differential ion pump and a turbomolecular pump allows for operating the chamber at any pressure range down to the 10^{-10} Torr range. It also considerably facilitates experiments when gas flow is required (i.e., in gaseous-surface interaction experiments). In addition, the turbomolecular pump allows for faster pumping after sample loading.

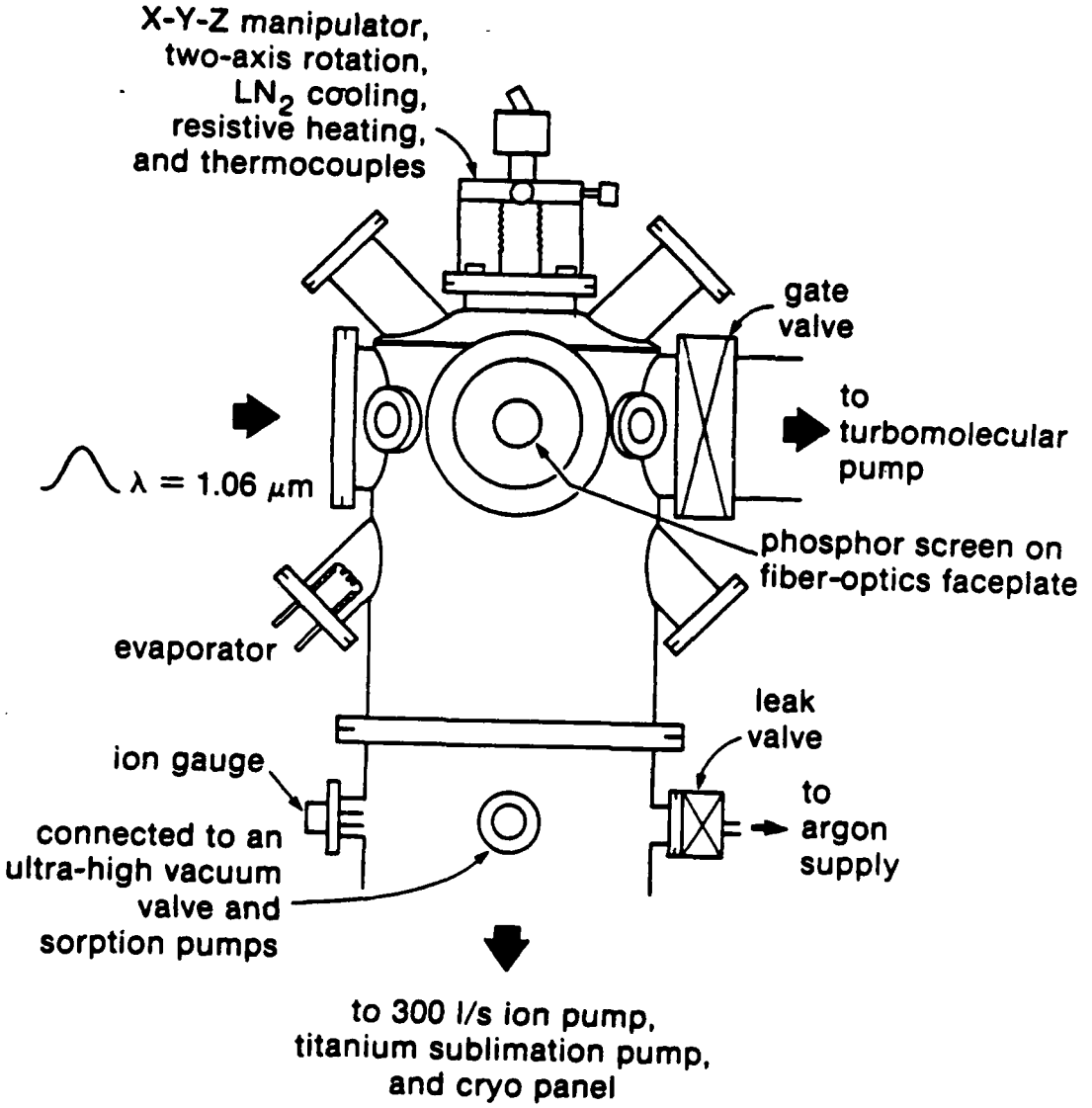

Fig. 2(a) A schematic diagram of the vacuum chamber (front view).

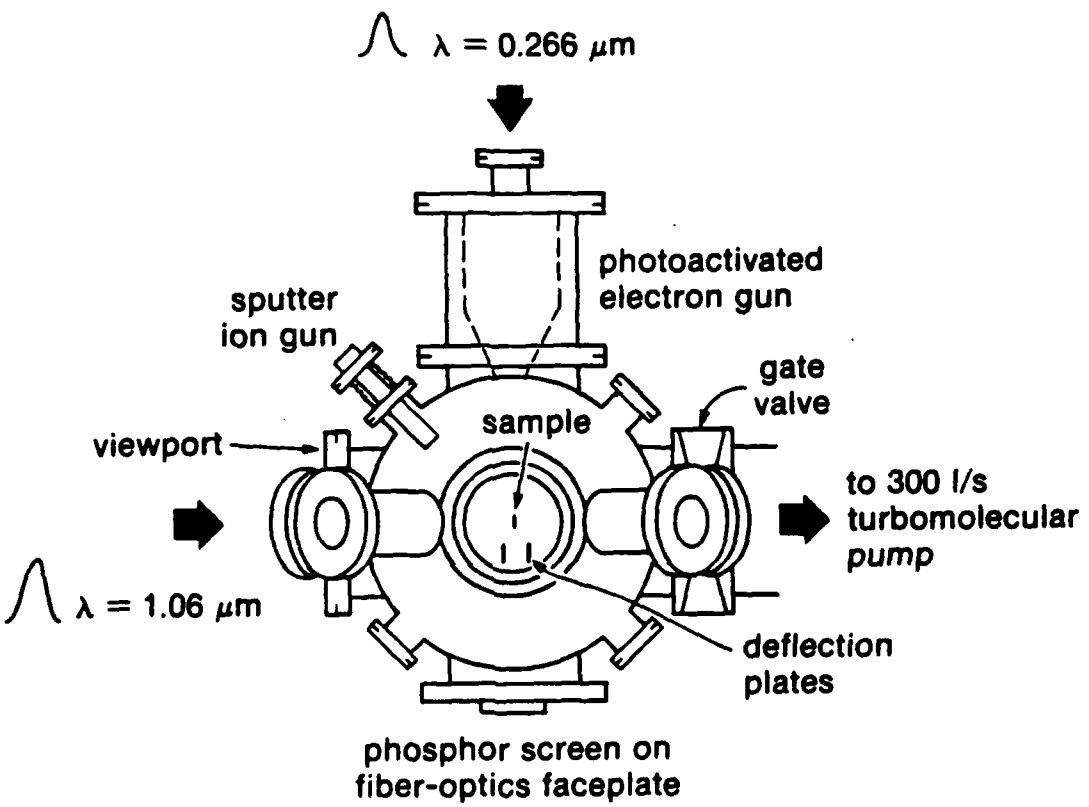

Fig. 2(b) A schematic diagram of the vacuum chamber (top view).

The sample is held on an X-Y-Z manipulator which provides two-axis rotation, liquid nitrogen cooling and resistive heating up to ~850°C. Temperature is measured by two thermocouples which can be attached to different locations on the sample. The usual crystal cleaning operation by argon ion bombardment and thermal annealing can be performed insitue.

The photoactivated RHEED electron gun is mounted on a 6" ID port opposite the phosphor screen which is deposited on a fiberoptics faceplate assembly. A pair of deflection plates is located between the sample and the phosphor screen and is used to position the primary and the diffracted beams on the screen.

IV. PHOTOACTIVATED ELECTRON GUN

The picosecond photoactivated electron gun was designed and fabricated at our laboratory. It is similar in design to a conventional pinhole x-ray streak camera. A schematic diagram of the gun and a picture of it are shown in Figs. 3 and 4. The photocathode was ~250 Å gold film deposited on a sapphire window by conventional evaporation techniques. This window was placed in a photocathode support electrode countersunk by the thickness of the sapphire window. Electric contact to the gold film was made by a layer of silver paint. After hardening of the silver paint, the photocathode assembly was thoroughly degassed by baking it inside a separate high vacuum system.

Gold was used as the material for fabricating the photocathode because it does not oxidize in air, which significantly simplifies the construction and operation of the gun. The photoelectric work function of gold is ~4.82 eV which is about equal to the photon energy of the frequency quadrupled Nd:YAG (4th harmonic $\lambda \approx 0.266$ μm, ~4.77 eV). Any adsorbed species or contamination lowers the work function. This allows us to use frequency quadrupled Nd:YAG to photoactivate the cathode. The small energy difference between the work function and the energy of the exciting photons is advantageous for the production of a near monochromatic electron burst. Because of the low primary electron

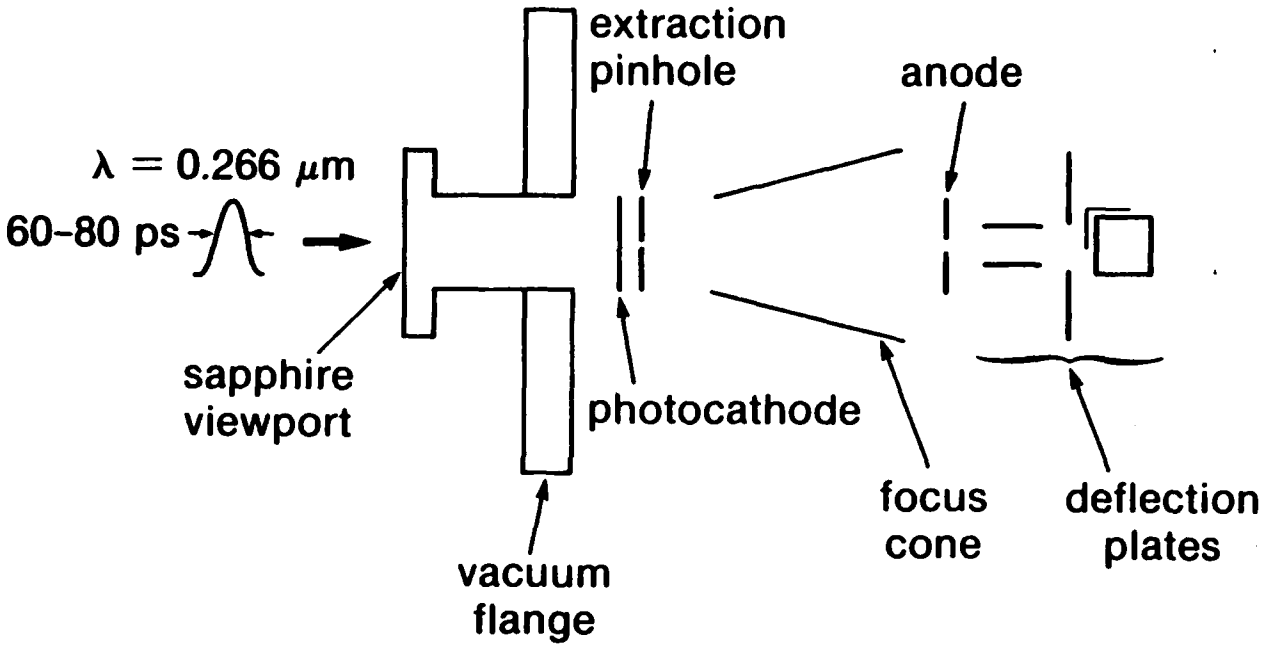

Fig. 3 A schematic of photoactivated picosecond electron gun.

energy, only electrons up to perhaps the second monolayer from the gold surface can escape to vacuum. Since the photocathode is used in a transmission mode, in principle, thinner gold films have better efficiencies. The choice of 250 Å thickness was made in order to assure good conductivity across the film and increase ruggedness. Throughout our work, we have used gold thicknesses varying from 150–300 Å. Typical photocathodes of 200–250 Å were found to be rugged enough to withstand months of operation with repeated exposure to the atmosphere.

A circular aperture of 0.25 mm diameter was located 1 mm from the photocathode and served as an extraction pinhole. The extraction electrode was followed by a focus electrode and an anode. A set of deflection plates and an electrode used for correcting astigmatism followed the deflection plates. The location of the various electrodes could easily be changed by changing the length of the machinable ceramic spacers between them.

The frequency quadrupled Nd:YAG pulse energy was less than one microjoule per pulse. The number of electrons per pulse was obtained by Faraday cup measurement of the electron current while the system is operated at 1 kHz repetition rate. The current collected by the Faraday cup, and thus the number of electrons per pulse, was found to be directly proportional to the ultraviolet intensity incident on the photocathode as shown in Fig. 5. These results indicate that no photocathode saturation is occurring for our experimental conditions. The absolute measurements of the number of electrons in each pulse was dependent on the photocathode lifetime and was strongly dependent on the angle of incidence and alignment of the exciting UV laser on the photocathode film.

In spite of no observable saturation in the electron current with ultraviolet photon intensity, measurement of the electron pulse width has shown that it is dependent on the laser energy. The electron pulse width measurement was conducted using a set of deflection plates in a streak mode as shown in Fig. 6. An FET high-voltage pulser capable of delivering 2.5 kV pulses with a rise time of 6 ns was used to drive the deflection plates. A detailed description of this FET high-voltage pulser will be given later. A digital delay

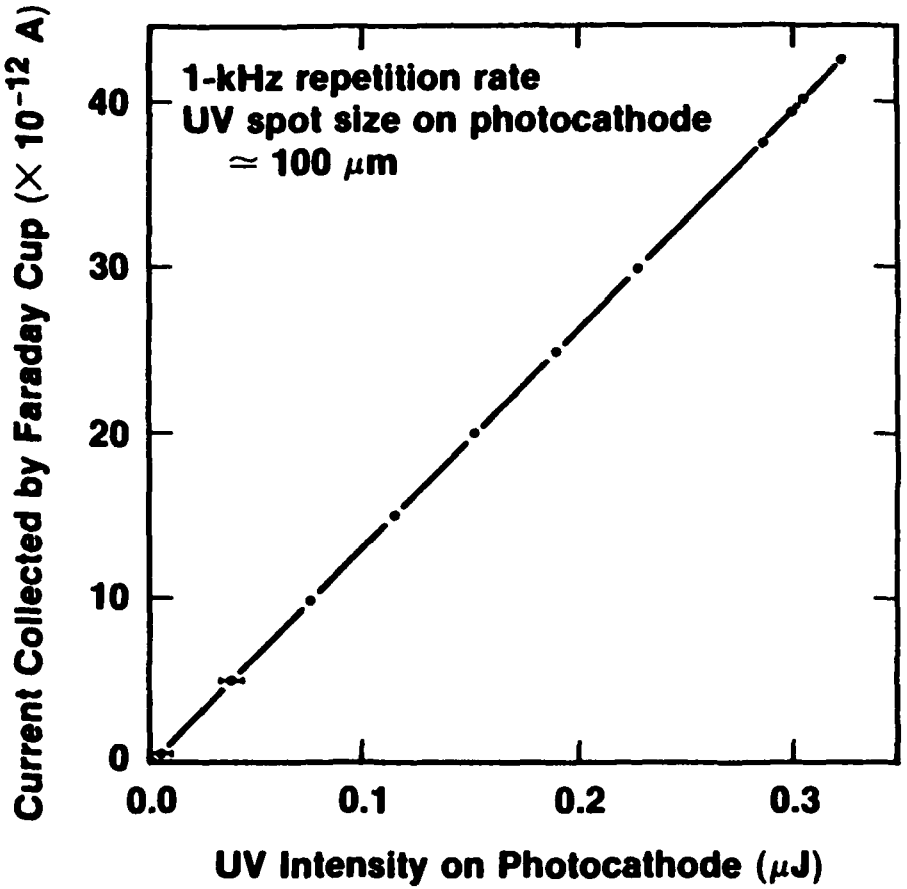

Fig. 5 Faraday cup measurement of electron current in the picosecond electron diffraction system.

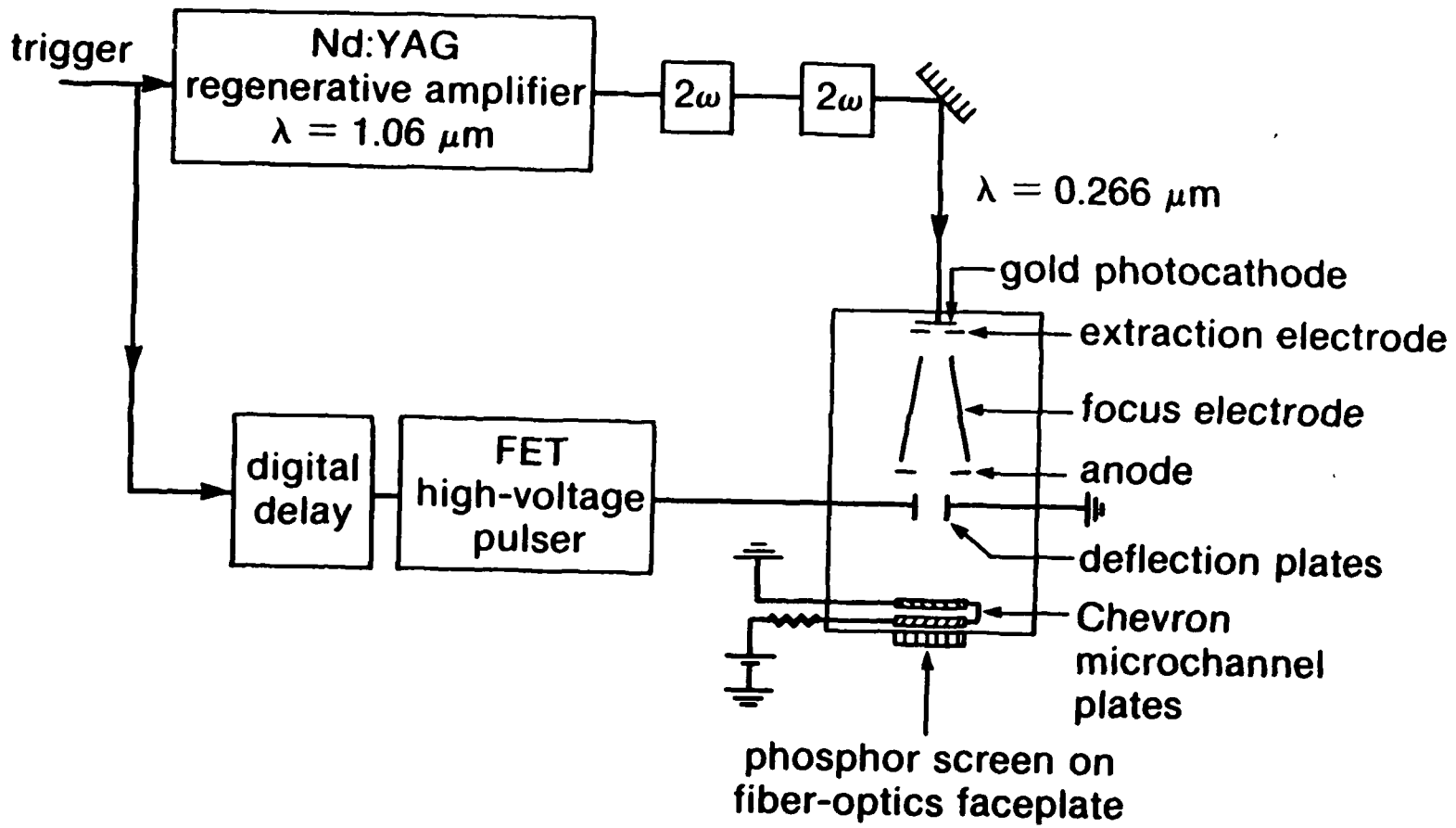

Fig. 6 Electron pulse-width measurement using deflection plates in a streak mode.

generator triggered the FET circuit after a set delay from the laser pulse. The mean jitter between the high voltage pulse and the laser pulse is 50 ps. Calibration of the sweep rate and checking for its linearity was accomplished by recording the streaked electron pulses at different delay settings. For such measurements the system was run at 1 kHz repetition rate. Thus, jitter between the high voltage pulses and the electron pulses results in an apparent broadening of the electron pulse since many pulses are averaged using a film in contact with the fiber optics faceplate.

Results of our measurements of the electron pulse width dependence on ultraviolet pulse energy are shown in Fig. 7. Clearly the electrons are broadened with the increase in UV intensity incident on the photocathode. This is known to be due to space-charge effects occurring near the photocathode or after the extraction pinhole. All measurements were made by photographically recording the streaks, digitizing these images on a microdensitometer, then obtaining linescans throughout them. Figures 7(a) and 7(b) were obtained using a single electron pulse. For Fig. 7(c) several pulses were averaged in order to obtain enough electrons to give a smooth streak. The FWHM of the electron pulse observed in Fig. 7(c) was measured to be ~160 ps. Given that there is an estimated 50 ps mean jitter between the high voltage pulse applied to the deflection plates and the laser pulse, then, the minimum electron pulse width obtained in these experiments was ~110 ps. This is larger than the 60–80 ps ultraviolet laser pulse since some initial broadening occurs due to variations in the energy and direction of the photogenerated electrons and due to jitter between the electron pulse and the laser pulse as a result of voltage fluctuations in the electron gun.

Such space-charge broadening of the electron pulse is strongly dependent on the field near the cathode and the extraction pinhole. Measurements shown in Fig. 7 were taken for a field of ~20 kV/cm applied between the photocathode and the extraction pinhole. The cathode in this case was biased at -25 kV. Raising the electric field between the photocathode and the pinhole and in the region after the extraction pinhole is expected to

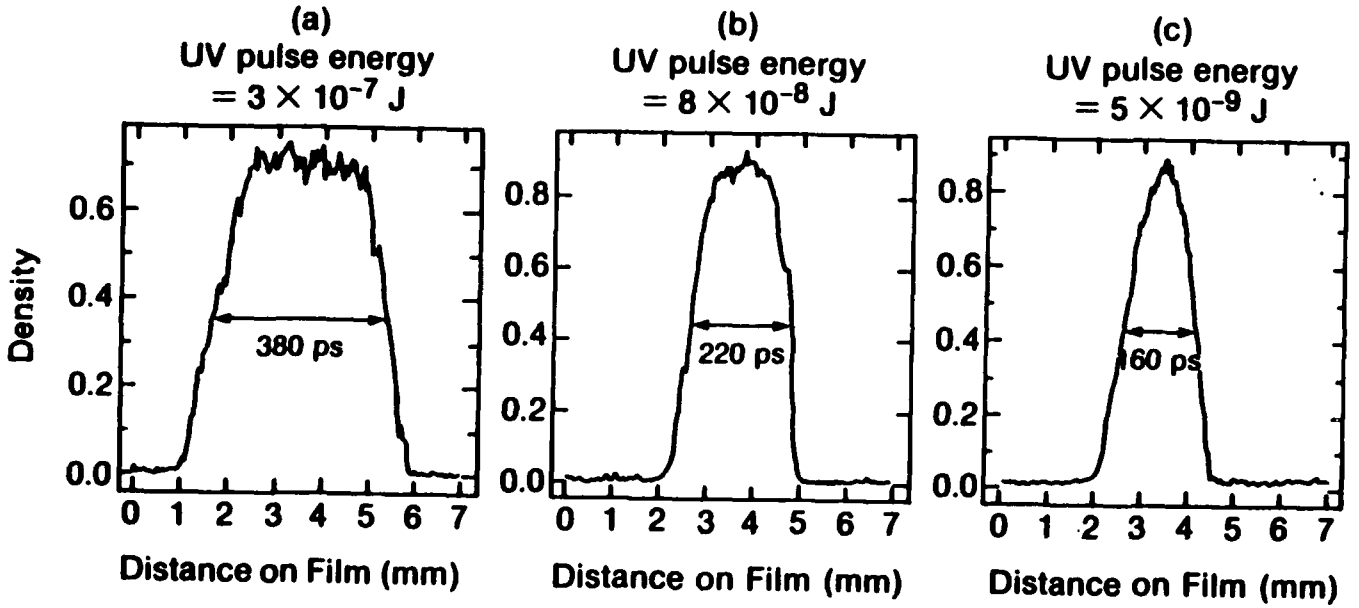

Fig. 7 Electron pulse width dependence on ultraviolet pulse energy.

reduce such space-charge broadening effects. No parametric study was conducted to minimize such space-charge effects. Extension of the present techniques to a few picoseconds, or even subpicosecond, resolution is possible by using shorter laser pulses to drive the photocathode and by minimization of electron temporal broadening.[26,27]

V. LASER SYSTEM

The laser system used to drive the picosecond RHEED apparatus is based on a Nd:YAG regenerative amplifier.[28] A schematic diagram of this system is shown in Fig. 8. A cw pumped mode-locked Nd:YAG oscillator generates a 100 MHz train of 120–160 ps pulses at a wavelength of 1.06 μm. A switch-out consisting of a Pockels cell and two polarizers is used to select a pulse at a variable repetition rate up to 1.5 kHz. This injection switch-out is used to protect the oscillator from feedback which would otherwise adversely affect its mode-locking, thus reducing pulse stability.

The oscillator pulse selected by the Pockels cell is coupled to a single mode optical fiber, in order to vibrationally isolate the oscillator from the amplifier, and is then coupled to the cw pumped regenerative amplifier by a wedge with ~4% reflection. The low reflectivity of the wedge protects the optical fiber from damage by the output of the regenerative amplifier. The injected pulse typically has an energy of a few picojoules. Pulse injection is accomplished by applying a fast step to the Pockels cell in the regenerative amplifier cavity[29] The magnitude of this voltage step is to achieve quarter wave retardation. This causes a cavity round trip of full wave retardation, thus minimizing cavity losses and trapping the injected pulse. After ~40 round trips, the pulse inside the regenerative amplifier cavity builds up to its peak value and is cavity dumped by applying a second step function causing the Pockels cell to have half wave retardation.[29] The build-up of the pulse inside the regenerative amplifier cavity and its dumping is shown in Fig. 9. This was observed by monitoring the leakage out of one of the cavity mirrors.

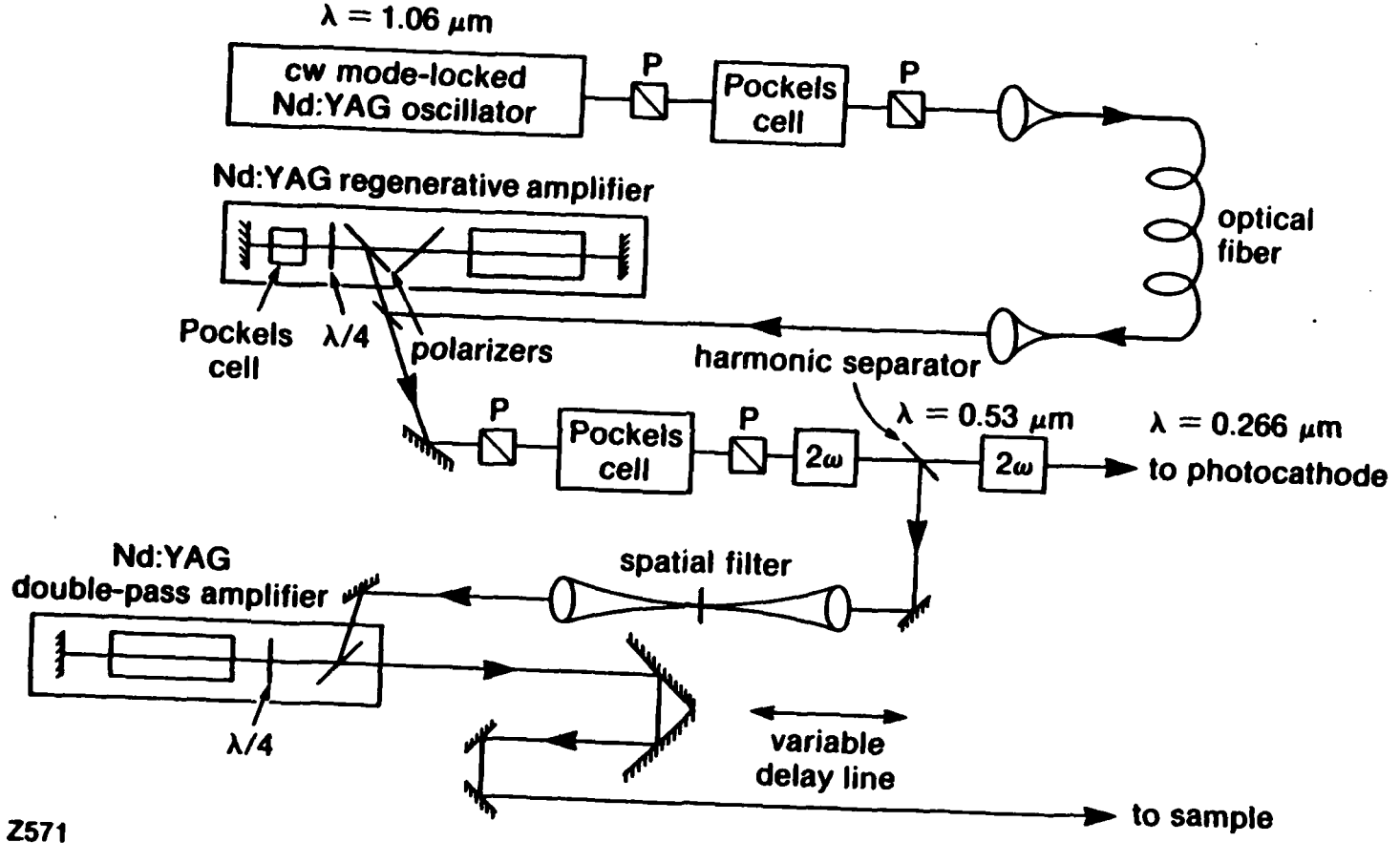

Fig. 8 Schematic diagram of the laser system.

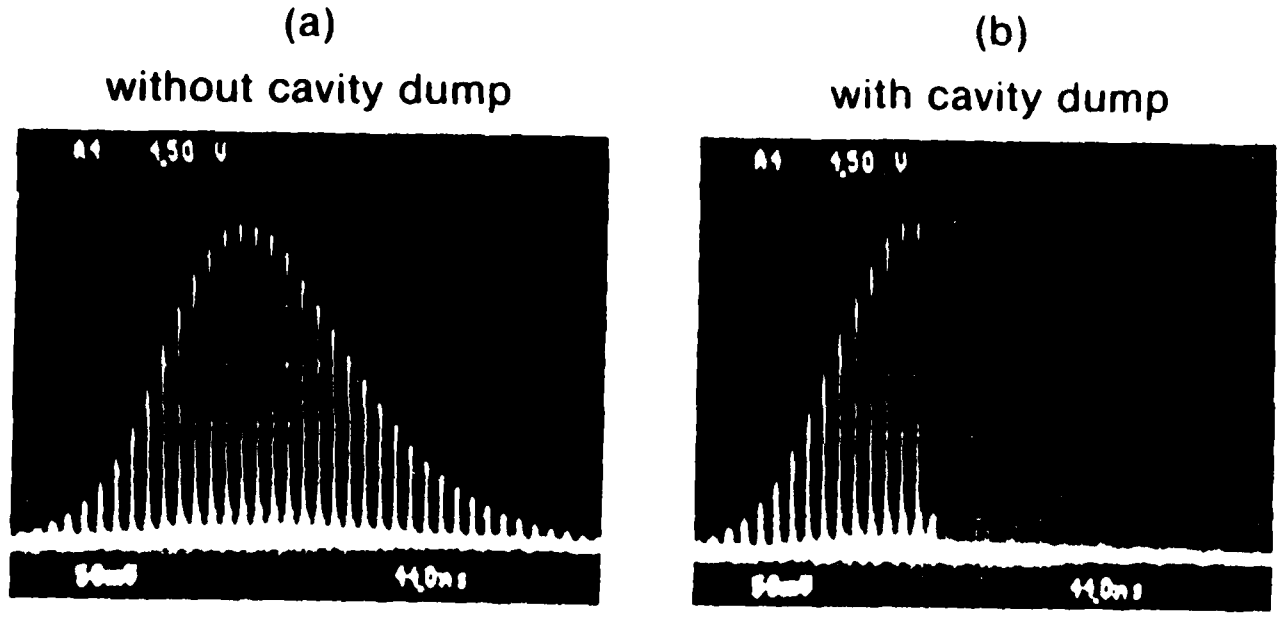

Z697

Fig. 9 Pulse buildup inside the regenerative amplifier.

The energy content of the principle pulse is typically ~0.4 mJ. The ratio of the energy content of the principle pulse to others is limited by the thin film polarizer in the cavity which is at best 300 to 1. Typically, this ratio is significantly less due to the acousto-optical properties of the $LiNbO_3$ Pockels cell currently used. To increase this energy ratio, an external switch-out consisting of a Pockels cell and two polarizers is used. The output of the regenerative amplifier before and after the external switch-out is shown in Fig. 10. After this external switchout, the energy content of the principle pulse to others is observed to be better than several hundreds to one.

The repetition rate of this system can be varied from a single shot to 1.5 kHz with shot-to-shot stability better than 5%. Such high stability is a consequence of the cw pumping of the regenerative amplifier.

The output of the external Pockels cell is frequency doubled in a KDP crystal. Only a few percent conversion efficiency is necessary. The fundamental and the frequency doubled Nd:YAG pulses are split in a harmonic separator. The green ($\lambda = 0.53$ μm) pulses are further doubled in a KTP crystal to generate ultraviolet pulses ($\lambda = 0.266$ μm). These ultraviolet photons are utilized to pump the thin gold film which is used as the photocathode in the picosecond electron gun.

The fundamental pulse is spatially filtered and passes through a 7 mm double-pass amplifier. When the high repetition rate mode of operation is desired, the double-pass amplifier does not get activated. In this mode of operation, a maximum of 0.3 mJ per pulse can be delivered to the sample. For single shot experiments, and when higher laser energies are needed to be delivered to the sample, the double-pass amplifier is activated. This produces a maximum of 30 mJ at 8 Hz repetition rate. An optical delay line is used to vary the timing between the fundamental pulse, which is used for sample heating, and the ultraviolet pulse which derives the photocathode.

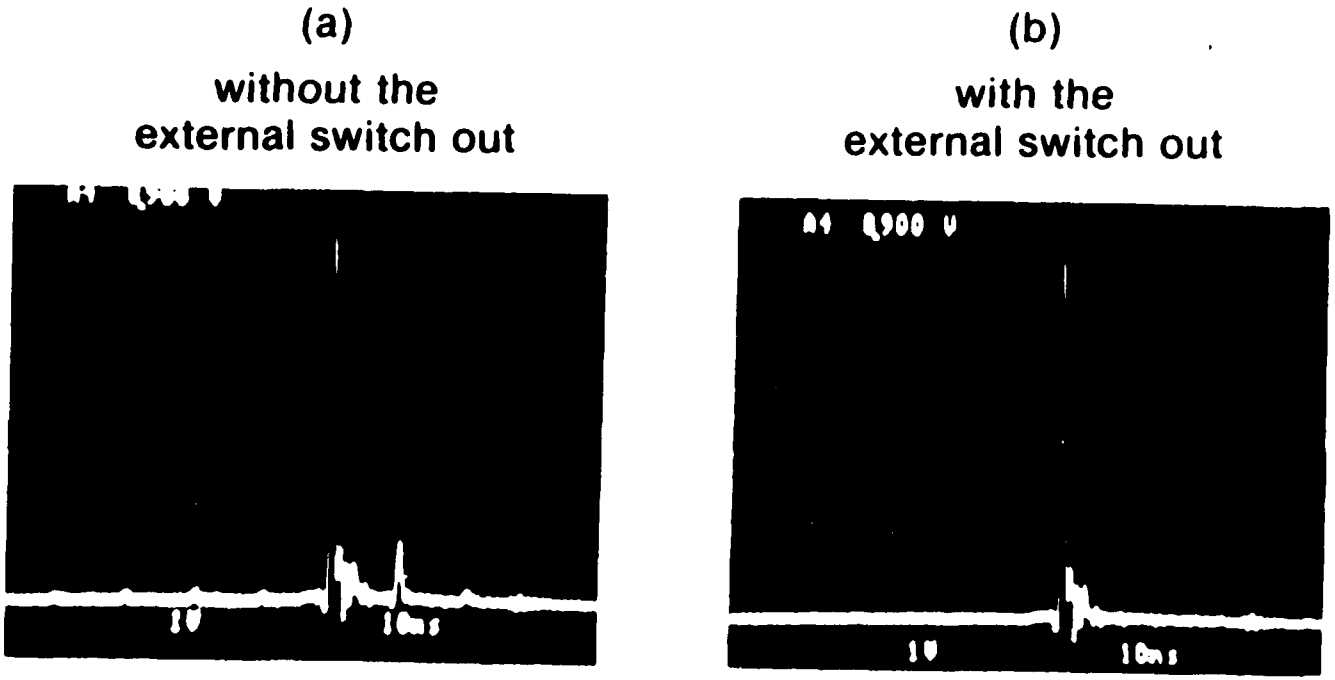

Fig. 10 Output of the regenerative amplifier: (a) without external switch-out and (b) with the external switch-out.

VI. ELECTRON DETECTION

(A) Detection System

Electron detection techniques used in conventional continuous electron diffraction apparatus (i.e., fluorescent screen or a Faraday cup) can be used for detecting the picosecond diffraction patterns. A key consideration in a picosecond diffraction apparatus is the efficiency of electron detection. This should approach the possibility of single electron detection if a single shot will be utilized. When the system is used is a repetitive mode, then this requirement is considerably relaxed depending on the number of pulses used to construct each diffraction image. In the current picosecond diffraction apparatus we are utilizing a detection system based on a phosphor screen deposited on a fiber optics faceplate. The fiber optics faceplate provides a one-to-one imaging of the diffraction pattern. Currently we are utilizing a P-47 phosphor which has a persistence time (decay time to 10% peak value) of 0.15 μs. This allows for high repetition rate operation which is advantageous for studying recurrent events as in simple surface lattice heating and cooling or in some surface phase transformations (e.g., surface reconstruction of Si). The presently used P-47 phosphor which fluoresces mainly in the blue, is somewhat less efficient than other slower phosphors.

For single shot or low repetition rate operation, the pattern has be be amplified. This is accomplished by inserting an image intensifier external to the vacuum chamber to amplify the light emitted by the phosphor. In an alternative approach, microchannel plates (MCP) are placed inside the vacuum chamber in proximity of the phosphor screen in order to amplify the electron diffraction pattern.

During experiments involving high intensity laser irradiation of the target, the surface or the target, or part of it, could evaporate and could emit ions. This introduces a strong ion signal following the electron diffraction signal. Such signal is delayed by the ion drift time from the target to the MCP. An example of this situation is shown in Fig. 11 where a thin aluminum film (~250 Å) was irradiated with the fundamental (λ = 1.06 μm)

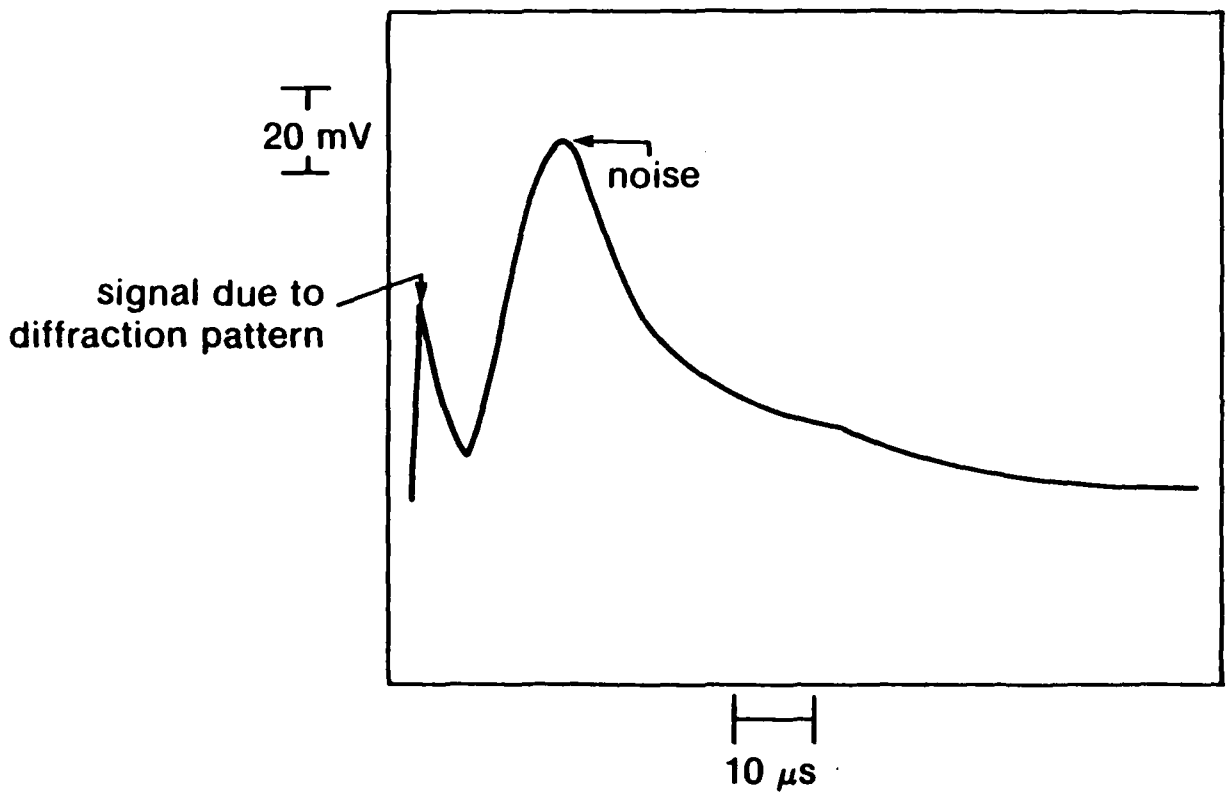

Fig. 11 Phosphor screen output detected by a photomultiplier during laser damage of a thin (~250 A°) aluminum film.

with a fluence above its damage threshold while the diffraction pattern of this film was also obtained. In this case, the delay between the heating pulse and the electron probing pulse was set such that the electron pulse arrives at the target before the laser. Clearly, if the MCP is not gated this ion signal will totally saturate the photographic film in contact with the fiber optics faceplate. Gating of the microchannel plates also reduces the background noise (dark noise, scattered electrons in the chamber, etc.) and results in an increased MCP lifetime.

(B) Microchannel Plate Gating

When microchannel plates are used in our experiments, they are gated such that they remain active for a short period of time (~20 ns) during which the pulsed diffraction pattern arrives at the MCP. Because of its wide application in high-speed atomic, plasma, and radiation physics, there is considerable interest in developing fast gating techniques for MCPs.[30,31] In principle, the physical limitation on the gating time of a microchannel plate is given by the electron transient time in the channel. This currently limits MCP gating time to ~100 ps[31] which is much shorter than that required for achieving our objectives. To reach subnanosecond gating time, it is necessary to construct the MCP electrodes as part of a transmission line with a characteristic impedence matched to that of the pulse generator output. Subnanosecond operation of up to 15 mm MCP area has been demonstrated.[30]

We have developed a simple FET circuit capable of producing high voltage pulses of up to 2.5 kV with a few tens of nanoseconds FWHM. This circuit was utilized in gating a chevron (two MCPs is series) assembly with a 40-mm area. The high voltage pulse was directly applied to the MCPs (i.e., without incorporating the MCPs in a transmission line). The gating time was accurately determined by an electron sampling technique and was found to be ~30 ns for a blocking ratio better than 3000:1.

1. Field Effect Transistor High Voltage Pulses

A schematic diagram of the high voltage pulses used in MCP gating is shown in Fig. 12. The principle of the design of this circuit is similar to that previously constructed for fast pulsing of Pockels cells.[29,32] In this circuit, one IRF840 FET drives the primary windings of four trigger transformers. The IN6263 diodes on the primary windings are to protect from ringing. The secondary winding drives four IRF510 FETs used as current amplifiers for triggering the high voltage FETs (BUZ50 Seimens). This current amplifying stage is needed since the secondary winding of the transformers do not provide enough current to drive the high voltage FETs. The bias for the drain of the current amplifying FETs is provided by a 62 volts zener diode. A variable applied voltage (700 V to 2.5 kV) is dropped across four stages of high voltage FETs, each consisting of two BUZ50 Seimens connected in parallel. When the circuit is triggered, the high voltage FET stages are activated sequentially and a high voltage pulse shows on the MCPs. The chevron MCP assembly was measured to have an input capacitance of ~50 pF. The 50 Ω resistor connected across the gate and the drain of each FET stage is used to sustain the drain current. The inductance, L, is used to bring down the voltage on the MCP. This results in a high voltage pulse applied to the MCP.

The high voltage pulse applied to the MCP has a width that depends on the applied voltage and is reduced at higher voltages. Figure 13 shows the open circuit high voltage pulse and when applied to the MCP. The peak amplitude of the voltage applied to the MCP was ~1650 volts. For these conditions the pulse FWHM was 45 ns. Repetition rates as high as 1.5 kHz could be applied. Our repetition rates are limited by the performance of the driving laser system and by the MCP dead-time (time needed for the MCP to replenish its charge).[33] The repetition rate of the high voltage pulser, however, is significantly higher since it is limited by the high voltage current supply and the biasing time constant (set by the FET gate capacitor and the 1 MΩ current limiting resistor).

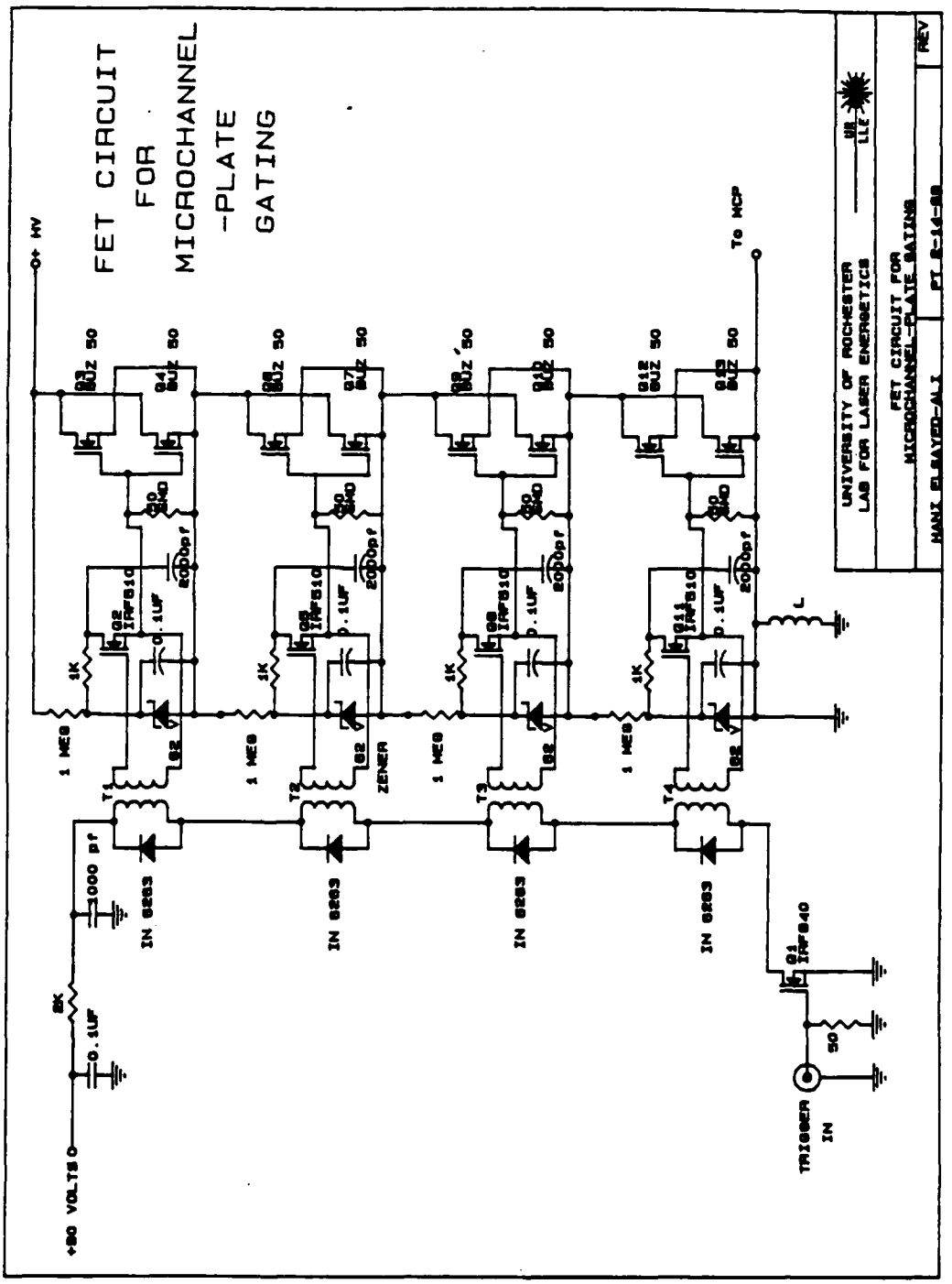

Fig. 12 FET circuit for microchannel plate gating.

(a)

(b)

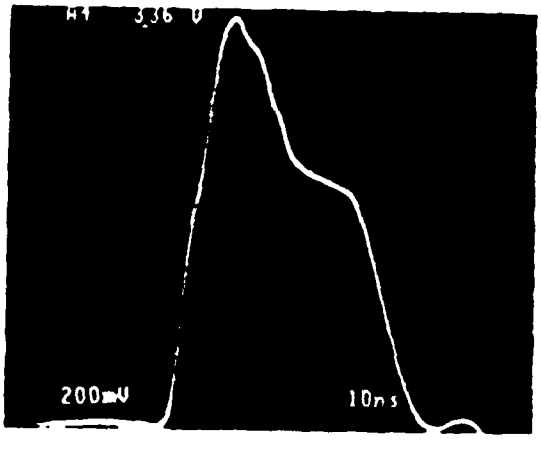

Z695

Fig. 13 Voltage output of the FET circuit for microchannel plate (MCP) gating. (a) Open circuit output; (b) Circuit connected to MCP. The high voltage probe used in this measurement is a 1:1166 divider.

2. Measurement of gating time

In order to measure the performance of this gating technique we used the picosecond electron gun as an electron sampling probe. The setup for measuring the MCP gating time is shown in Fig. 14. In this measurement, the frequency quadrupled Nd:YAG laser (λ = 0.266 μm, 60–80 ps FWHM) is driving the photocathode in the usual manner. The voltage applied to the focus cone, however, is set such that the electron pulse is defocused and fills the entire MCP area. The MCPs are drived by the FET high voltage pulser which is synchronized with the laser pulse. A variable delay circuit is used to set the timing between the high voltage pulse applied to the MCPs and the electron pulse. Since the electron pulse is much shorter than the gate width and since the jitter between the high voltage pulse and the electron pulse is estimated to be less than 100 ps, an accurate measurement of the gating time can be obtained by scanning the digital delay while observing the output of the photomultiplier. Results of such measurements are shown in Fig. 15. In this case the system was running at 1 kHz repetition rate. Results show a gate profile with FWHM of 10 ns. This is narrower than the applied high voltage pulse since the response of the MCP is highly nonlinear with the applied voltage.[33] The MCP gain drops to less than 0.0003 of its peak value 15 ns after the peak. This gives a gate width of ~30 ns for a blocking ratio better than 3000:1. A blocking ratio better than 10000:1 is achieved for a gate width of ~50 ns. Such performance was more than adequate for our objectives.

VII. SYSTEM OPERATION

The kilohertz repetition rate available from the regenerative amplifier considerably facilitates the alignment of both the laser system and the electron diffraction system (i.e., crystal and electron beam alignment). Experiments, however, are typically conducted at the low repetition rate (8 Hz) since laser fluences of several millijoules are needed for sample heating. This requires the operation of the double-pass amplifier which limits the repetition

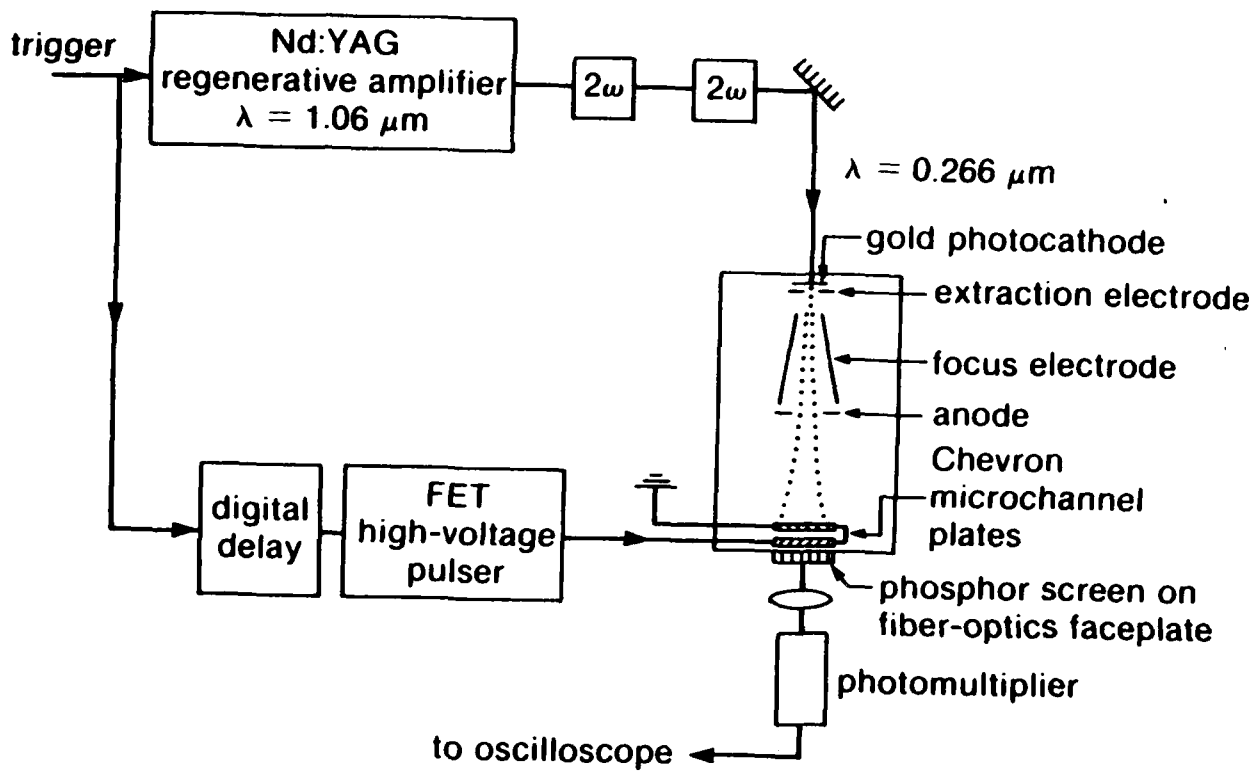

Fig. 14 Experimental setup for measurement of microchannel plate gating time.

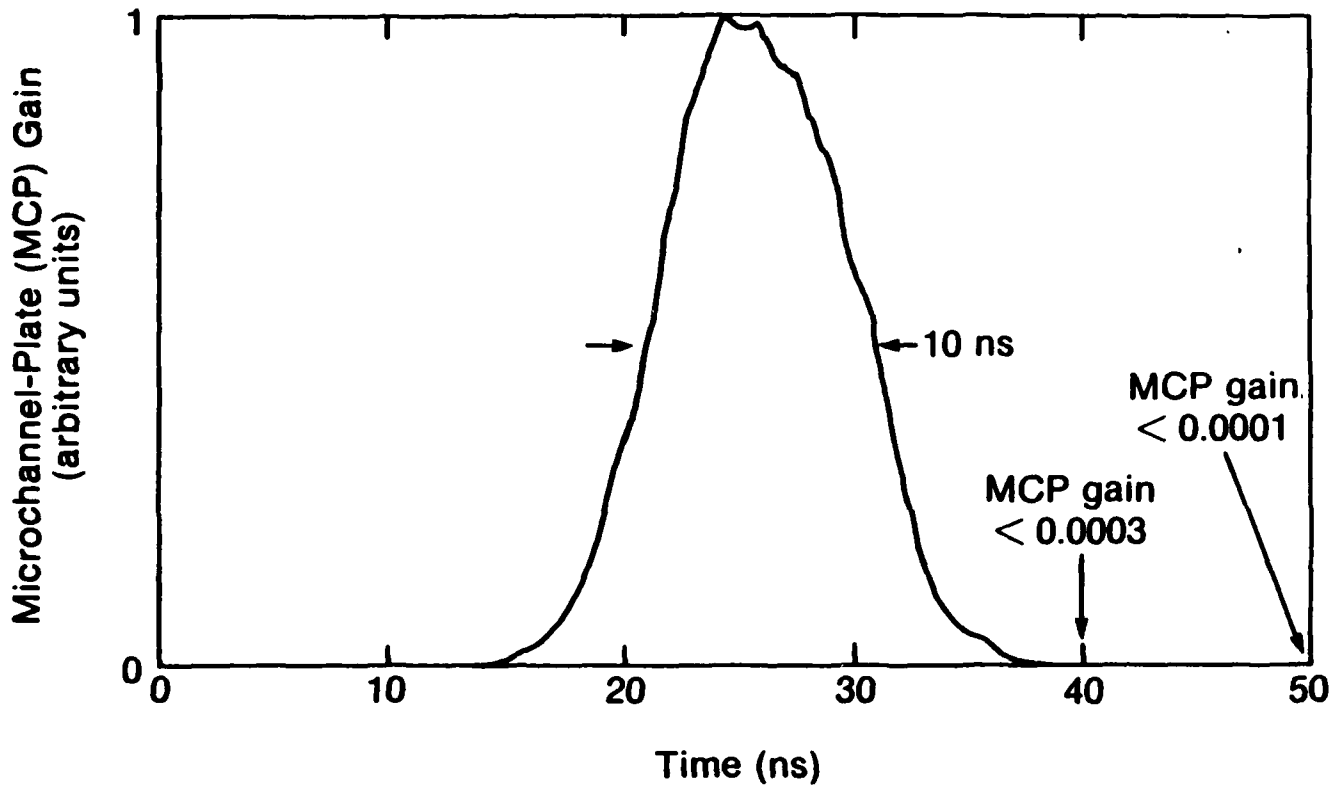

Fig. 15 Microchannel plate gating time.

rate. For studying reversible reactions (as in the case of simple heating), we take advantage of multiple-shot averaging in order to enhance our statistics. For nonreversible transformations, single-shot operation can be utilized. Figure 16 shows a diffraction pattern of Pb (110) crystal with the electrons aligned along the [110] direction for a single-shot and 20 shots. Chevron microchannel plates were used to amplify the diffraction pattern. The microchannel plate gain was, however, significantly reduced when twenty shots were averaged [i.e., in Fig. 16 (b)]. The electron pulse width (FWHM) for these experiments was ~300 ps. From Fig. 16(a), we see that a single electron pulse with FWHM of a few hundred picoseconds is sufficient to produce a good RHEED pattern.

For reversible events it would be advantageous to average several shots or even to remove the microchannel plates and average thousands of shots. The maximum repetition rate of this system when no microchannel plates are used is limited only by the laser repetition rate since the decay time of the phosphor screen (P-47) is ~150 ns. When microchannel plates are used the maximum repetition rate is limited by their dead time (time needed to replenish the charge) which typically limits the system to a few kilohertz.[33]

VIII. SURFACE MELTING

The technique of picosecond time-resolved reflection high-energy electron diffraction is most suitable to study ultrafast surface reactions (physical or chemical) in addition to its utilization as a picosecond time-resolved lattice temperature probe. Perhaps the most fundamental surface phase transformations associated with simple heating are surface melting and reconstruction. By surface melting we mean the melting of the top few monolayers at a temperature below the bulk melting temperature. Although very little studies have been done to understand the dynamics of these transformations, evidence exists that these phase transformations can proceed with extremely high speeds. In fact, the existence of surface melting has been experimentally verified only a few years ago.[25] Several numerical simulations, however, have predicted the occurrence of surface

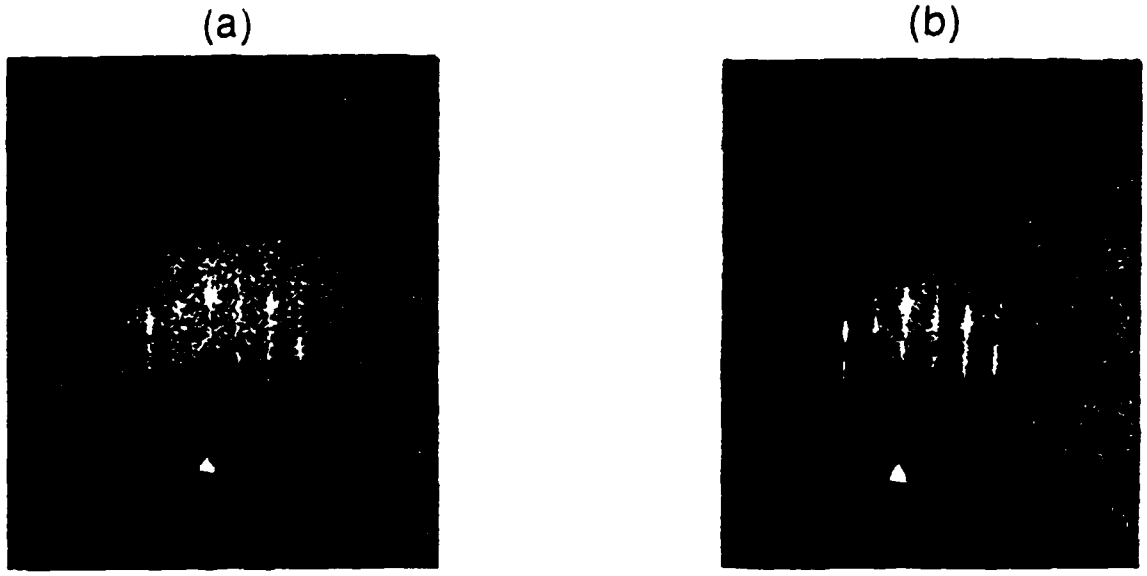

Z731

Fig. 16 Reflection high energy electron diffraction (RHEED) patterns of Pb(110) surface taken using the picosecond RHEED apparatus (a) using a single shot, (b) after averaging 20 shots and lowering microchannel plate gain. The electron pulse width ~300 FWHM and electron energy 14 kV.

melting.[34–37] In a molecular-dynamics simulation of the melting process of the Au (111) surface, it was shown that the outermost layers of the unreconstructed Au (111) surface melts ~100°K below the bulk melting transition. In these simulations, equilibrium conditions occurred in a time regime of ~10^{-10}S–10^{-9}S.[37] Thus, picosecond RHEED appears to be particularly suitable to study the dynamics of surface melting.

(A) Melting

Although melting is a most fundamental phase transformation that occurs upon heating a crystal to a sufficiently high temperature (which depends on pressure), a comprehensive microscopic theory of melting is not available. Indeed, many of the theories and experiments on bulk and surface melting are contradictory.[38–41] What is know about melting is mainly from a thermodynamics point of view. Melting is a first order phase transformation accompanied by a discontinuous change of entropy. At the melting temperature, the Gibbs free energy per mole of the bulk liquid is equal to that of the solid and the two phases coexist. While undercooling of liquids during solidification is a well documented phenomenon, evidence of superheating of solids could only be obtained under special c nditions and remains to be a controversial issue.[38,39]

In fact, currently there are two views of melting.[39] One view is that solids cannot be superheated. Since any order-disorder transformation should not require the nucleation stage, therefore, when there is sufficient energy, the disordering process could take place within the period of one vibration (~100 fs). Another view is that any transformation requires nucleation of some sort. For melting, this could be the nucleation of liquid drops, vacancies, dislocations, or some yet unidentified defects. Depending on the rate of these nucleation processes, a solid could be superheated to the extent necessary for the nucleation to take place.

If we adopt the view that melting proceeds by a nucleation and growth process, then the well documented absence of superheating under normal conditions could be

explained by the lack of an energetic barrier for nucleation. Such asymmetry between the melting and the freezing phenomenon, where no superheating is observed under normal conditions for the first, while large supercooling is easily observed for the second, is sometimes attributed to premelting phenomena (surface melting and roughening).

According to the Lindemann criterion,[42] melting occurs when the vibrational amplitude reaches a certain critical fraction of the interatomic distance (~10%). Since surface atoms have a reduced number of nearest neighbors, their instability temperature could be lower. That is, the surface melting temperature could be lower than the bulk. If the surface melts before the bulk, such a surface molten layer would provide a vast two-dimensional nucleus site for bulk melting. The existence of surface melting is consistent with the often valid relation:[39]

$$\gamma_{sv} > \gamma_{sl} + \gamma_{lv} \qquad (1)$$

where γ_{sv}, γ_{sl}, and γ_{lv} are the interfacial free energies per unit area of the solid-vapor, solid-liquid, and liquid-vapor interfaces. This relation simply states that it is thermodynamically more favorable to melt the surface when its temperature approaches the bulk melting temperature. Thus, for thermodynamically equilibrium conditions, this relation demands the existence of a microscopic liquid-like film between the solid and vapor phases at temperatures just below the bulk melting temperature. The surface melting temperature will depend upon the magnitude of this inequality.

(B) Evidence of Surface Melting

The earlier experimental evidence of surface melting was obtained by the observation of macroscopic properties near the bulk melting point. These included the strong increase in surface self-diffusion coefficient, changes in heat conductivity, heat capacity, and electrical conductivity near the bulk melting point.[38] Other indirect evidence of surface melting include the rotation of small zinc crystals on carbon,[43] morphology

changes of vapor inclusions in tetrabromnethan crystals near their melting point,[44] and the observation of the growth form of high-index planes of zinc from the vapor phase.[45] Further experimental evidence of surface melting comes from the observation of equilibrium forms of negative crystals (inclusions) of diphenyl.[46] In these experiments, it was observed that surfaces melted 10–20°K below the bulk melting temperature depending upon the nature of the surface (closed-packed surfaces melted only at the bulk temperature). More direct evidence of surface melting was obtained by the observation of the optical properties of copper near its melting point.[47] Perhaps the most definitive experiment demonstrating surface melting were those using ion-shadowing and blocking and using reflection high-energy electron diffraction to study the melting of the (110) surface of lead.[25] These studies have revealed that positional disordering of the surface region starts at ~0.75 of the bulk melting temperature. Another important experimental evidence was the low energy electron diffraction (LEED) observation that, for the (111) surface of germanium, the outermost layers lose lateral crystalline order in a continuous phase transition starting ~150°K below the bulk melting temperature.[48]

The existence of surface melting "premelting" as a consequence of relation (1) can explain the lack of observation of superheating under normal conditions. As the melt of most solids completely wet their parent solid at the melting point, such a liquid surface provides a vast nucleation site for the growth of the melt. However, for some materials relation (1) does not appear to be true. In this case, it is possible to externally superheat the solid. It appears that the surfaces of crystals of P-toluidine[49] and gallium[50] could be superheated without melting. This is consistent with the observation that gallium does not wet its solid.[39] Evidence of this nonmelting behaviors has been observed for few elements including cadmium and zinc.[51] In spite of these observations, attempts to study the kinetics of melting in gallium, for example, were unsuccessful since achieving a detectable superheating at the interface requires high melting rates.[39]

IX. RHEED STUDY OF SURFACE MELTING OF Pb(110)

We have conducted a RHEED study of surface melting of Pb(110). These studies were conducted using resistive heating. The goal of this work was to test the current experimental observations of surface melting, to provide an idea about the change in diffraction pattern with temperature, and to prepare for the time-resolved study.

The lead crystal (obtained from monocrystal at Cleveland, Ohio) was prepared by the Bridgman method in a pure graphite cruisable and had a purity ≥99.999. After its alignment, the crystal was mechanically sawed to give a disk of ~1.2 mm diameter and 2 mm thickness. The miscut angle was checked by Laue back reflection to be ≤1°. The crystal was polished on a glass plate to a mirror finish using various grades of silicon carbide, then it was chemically etched to remove the polishing damage. A standard solution was used for chemical etching[52] followed by rinsing in distilled water and quickly drying the crystal with dry nitrogen. This procedure was repeated just prior to installing the crystal inside the chamber. Insitue cleaning of the surface was accomplished by argon ion bombardment (1 KeV at 10^{-6} torr) while the sample was at 550°K. To assure annealing of surface damage, the sample was brought up to 580°K after argon ion bombardment was stopped. The temperature of the sample was measured by two thermocouples attached to the sample holder in close vicinity to the sample at the top and the bottom of the sample. Due to heat sinking at the top of the sample stage, there was a temperature gradient across the sample by ~6°K. An average value was used for our analysis since no effort was made to determine the exact location of the probing electron beam on the sample.

Two sets of data are shown in Figs. 17 and 18. The 14 KeV electron beam was incident along the [110] azimuthal direction. For these measurements, we have used the laser to drive the photocathode of the electron gun although no time-resolved data on surface melting were collected. To enhance the data collection rate, the electron gun was operated at a frequency of 1 kHz.

The diffraction patterns showed the usual RHEED streaks and spots. In addition to the background due to inelastically scattered electrons and Kikuchi bands and lines due to bulk lattice planes diffracting the inelastically scattered electrons. The appearance of Kikuchi bands and lines is indicative of crystal perfection. These lines are more clearly seen in Fig. 18 since for this set of data the crystal was annealed for a longer time and at a higher temperature.

Our observations appears to be consistent with that of Frenken et al.[25] As the temperature of the crystal was raised, there was a reduction in the intensity of the diffraction rods and spots. This is attributed to the surface Debye-Waller factor. No quantitative analysis was made to determine the surface Debye temperature. Beyond ~500°K, the rate of reduction in the diffraction intensity appears to significantly increase. At ~566°K, no diffraction spots or rods were observable. This observation indicates the long-range disordering of the few atomic monolayers which are probed by the electrons (~4 monolayers). In the experimental set of Fig. 18, for which the Kikuchi lines were strong, such lines were still observable even after the diffraction rods and spots totally disappeared. This indicates that the bulk order was maintained. The surface disordering (surface melting) was found to be reversible with cooling. In several cycles of heating and cooling, the same behavior was observed.

X. A PICOSECOND TIME-RESOLVED LATTICE TEMPERATURE PROBE

The use of ultrafast lasers (nonosecond to femtosecond) to study and alter surface properties and reactions has become a well established field of research. Ultrafast heating of surfaces with lasers offers a unique capability in terms of heating and cooling rates. These rates could approach 10^{11} K/s which is not accessible by other means. Such exceptionally high heating and cooling rates allow us the initiation of surface physical and chemical reactions that would not be favored at slower heating rates. For example, when a substance is adsorbed to a surface at low temperatures, heating of the substrate could result

in either its desorption or reaction with the substrate (e.g., oxygen on copper). Depending on the surface heating rate, the kinetic parameters could be made to favor one of the two possibilities. Typically, the higher heating rates would favor desorption.

In addition to altering the path of surface reactions by fast heating, the use of ultrafast lasers offers the capability of monitoring the intermediate product species and surface phases. This information is invaluable to the understanding of surface phenomena.

Tunable ultrafast lasers (particularly in the infrared part of the spectrum), offers a unique possibility of preferential excitation of the vibrational states of the adsorbed substance. The excitation rates could be fast enough that nonequilibrium conditions would exist (i.e., the relaxation time of the system is slower than the laser pulse width). Such nonequilibrium conditions could be exploited to produce unique surface reactions.

When resonant excitation of the adsorbed species is performed using a fast laser pulse, substrate heating could be produced by laser energy coupling to the vibrational states of the adsorbed species which could in turn effectively couple to the substrate. Thus, the desorption phenomena could be either (or a combination of) a photo-induced process and a thermal process.

In addition to the study of the physical and chemical properties of adsorbate/substrate reactions, ultrafast lasers could also be used to induce and probe other surface reactions as in the case of surface phase transformations (e.g., reconstruction, other diffusionless transformations, and diffusion initiated reactions). The fast heating rates offers the ability to probe the evolution of these processes and thus understanding their kinetics.

In the study of the interactions of ultrafast lasers with surfaces and the subsequent reactions, a key parameters is the time evolution of the surface temperature. Typically, this is determined for simple systems using a solution of the heat diffusion equation. But even for the simplest cases (e.g., simple heating of a substrate which undergoes no phase change), such a solution can provide the time evolution at the surface temperature with poor

accuracy since many assumptions are built in these models. These assumptions include the temperature behaviors of the specific heat of the laser irradiated material, its diffusivity, and laser energy coupling. It has been previously proposed that resonantly enhanced second harmonic generation at surfaces could be used as a surface temperature probe.[11,13] Although this has been demonstrated for Ag(110) surface heated with nanosecond laser pulses,[13] this approach does not offer a general technique suitable to time resolve the evolution of the surface temperature. Here we demonstrate the utilization of picosecond RHEED as a lattice surface temperature probe.

The sensitivity of the diffraction pattern to temperature was clearly demonstrated in the last section. This sensitivity comes from the fact that as the temperature is raised, there is an increased atomic vibrational amplitude and thus an increased dephasing of the atomic scattering centers. The effect of this dephasing on the diffraction pattern is to reduce the number of electrons elastically scattered (i.e., to reduce the diffraction rod intensity). The reduced rod intensity shows up as increased background which is due to inelastically scattered electrons. Such a reduced intensity occurs with no widening of the diffractional rods (or spots). This effect is known as the Debye-Waller effect and its theory was first developed by Debye for x-ray diffraction.

We have conducted a measurement of the surface Debye-Waller effect with a few hundred picosecond time resolution on a Pb(110) crystal. For these experiments the angle of incidence of the electrons was adjusted such that the diffraction conditions showed shortened streaks as shown in Fig. 19. The 1.06 μm fundamental was used to heat the surface of the sample while the electron pulses were used to probe the surface in the manner described previously. The system was operated at 8 Hz repetition rate. The laser heating pulse had an energy of ~11 mJ per pulse and a spot size on the sample of 1.1 cm FWHM. Thus there was some nonuniformity in the heating of the surface at the sample. The infrared heating pulse passed through a delay line before hitting the sample. Adjustments of the delay line provided the means by which the electron pulse arriving to

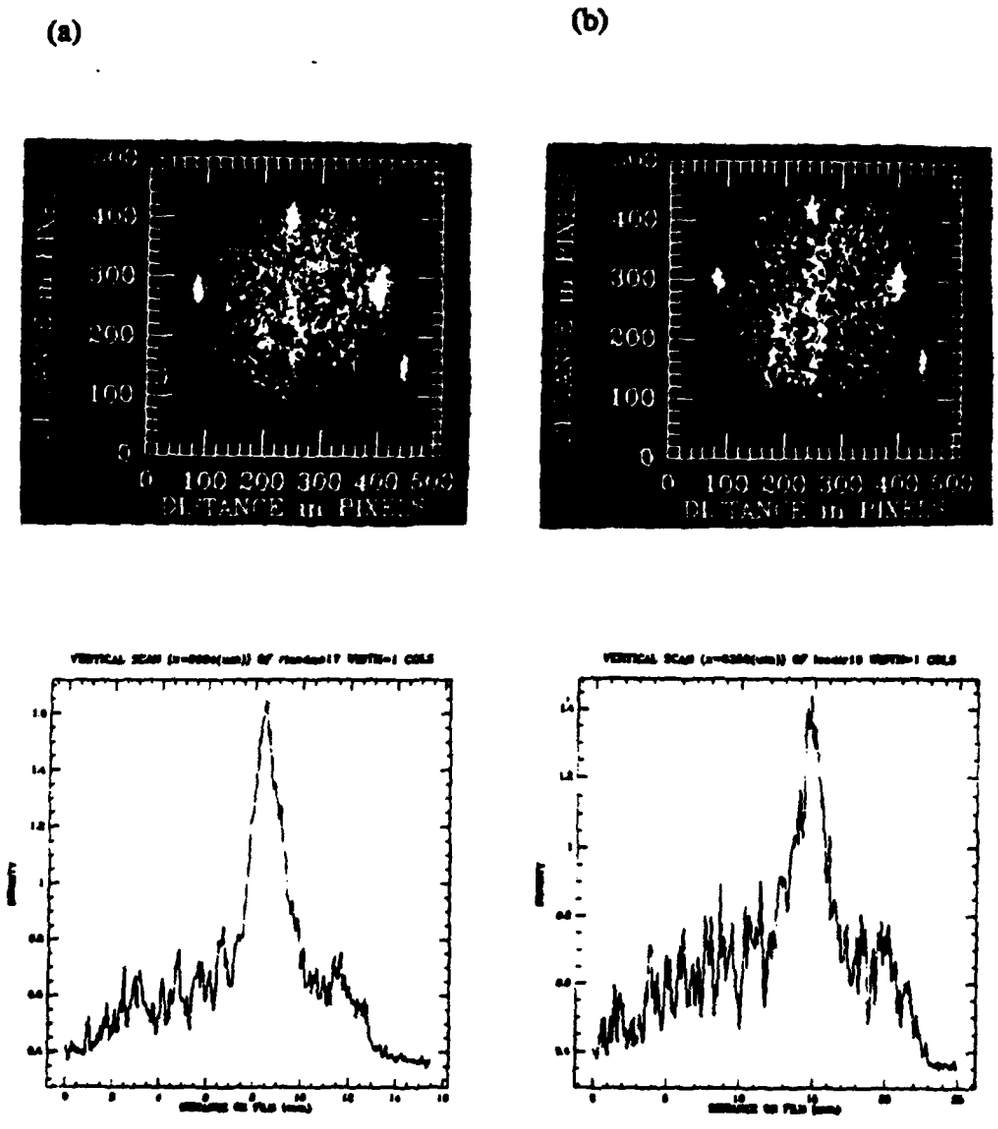

Fig. 19 RHEED patterns of Pb(110) obtained (a) without laser heating (b) ~2 ns after the laser heating pulse. The line scans were taken along the 02 diffraction rod.

the sample was delayed a set amount of time from the time the heating pulse strikes the sample. In order to enhance our signal, we averaged over a number of shots (80 shots). This averaging effectively compensated for shot-to-shot fluctuations, however, does not compensate for long therm drifts in the laser or in the electron gun. The effect of such long term drifts were minimized by obtaining a sequence of diffraction patterns without and with laser heating at each delay line setting.

The diffraction patterns were recorded photographically on a film in contact with the faceplate. The developed negative was then digitized on a microdensitometer and analyzed using standard image analysis routines. Line scans through the 02 diffraction rod were obtained as shown in Fig. 19. Many of these scans were made at different locations to assure that we recognize the scan through the highest film density. This process was repeated for diffraction patterns obtained without and with laser heating at various delay lines. For each film, the film density was converted into relative intensity using the relation:

$$\text{Density} \propto \log_{10} \text{Intensity}$$

Care was taken to assure that the film was operating at a regime satisfying the above relation. This was accomplished by taking several exposures with different number of pulses and comparing the produced film density.

Results showing the behavior of the 02 rod intensity as a function of the delay line setting are shown in Fig. 20. These were normalized to the intensity before laser heating. Clearly the cooling curve is obtained. This can be related to the lattice temperature through the surface Debye-Waller factor which can be obtained by static heating as was shown in the previous section. Cooling of the surface is shown to be almost complete in several nonoseconds as can be expected from a solution of the heat diffusion equation.

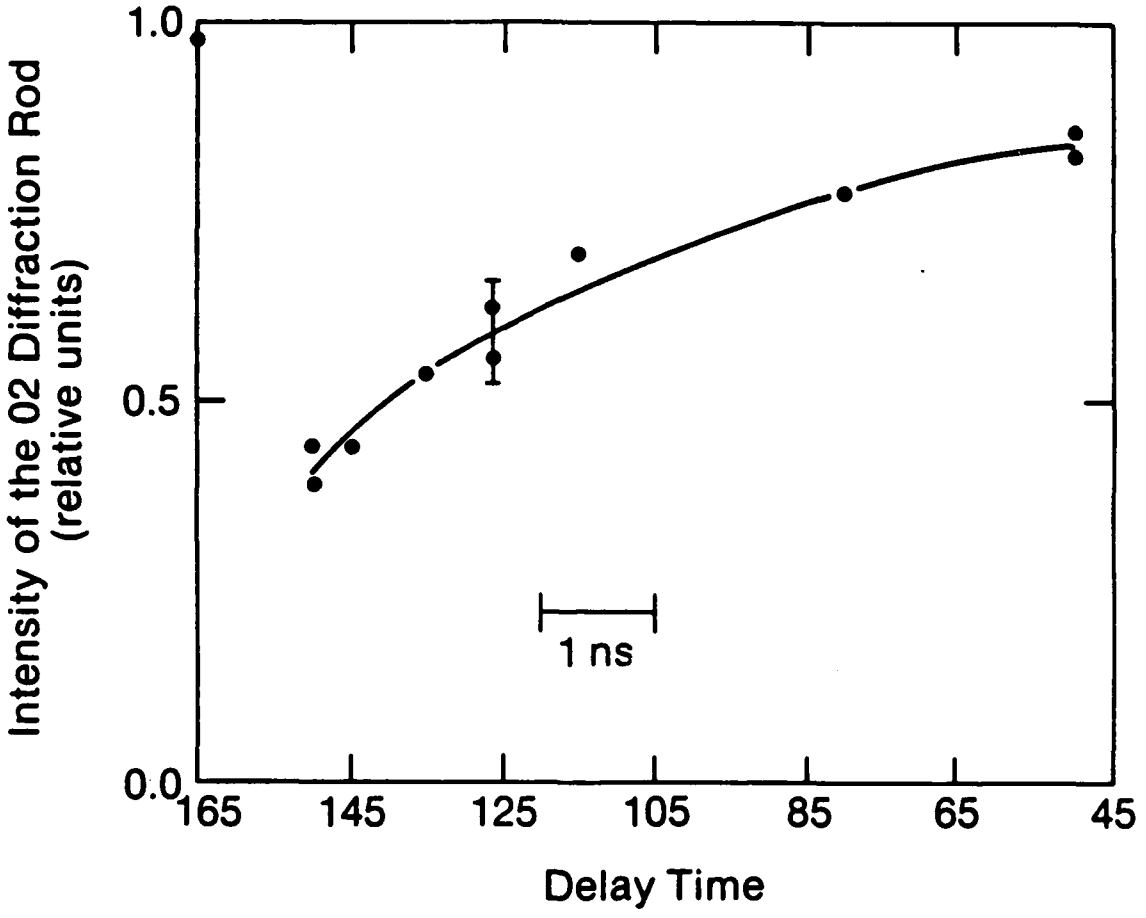

Z728

Fig. 20 Intensity of the 02 diffraction rod after laser heating. Values were normalized to that without heating (i.e., sample at room temperature).

XI. CURRENT PERSPECTIVES ON PICOSECOND RHEED

An ultrahigh vacuum picosecond electron diffraction facility was developed and characterized. With this facility, we are capable of monitoring the structure and temperature of surfaces with up to ~100 ps time resolution after laser irradiation. The use of this technique to probe surface lattice cooling after pulsed laser irradiation was well demonstrated. This provides a picosecond time resolved surface lattice temperature probe. Surface melting of Pb(110) crystal was demonstrated by using this apparture in a static mode of operation. Dynamic experiments to study the kinetics of surface melting are in progress.

XII. REFERENCES

1. For example, "Laser-Controlled Chemical Processing of Surfaces," edited by A. Wa Johnson, D. J. Ehrlich, and H. R. Schlossberg (North-Holland, New York 1987) Materials Research Society Symposia Proceedings, Vol. 29; Chemistry and Structural Interfaces: New Laser and Optical Techniques, edited by R. B. Hall and A. B. Ellis (VCH Publishers, New York, 1986).
2. J. M. Liu, H. Kurz, and N. Bloembergen, Appl. Phys. Lett. 41, 643 (1982).
3. C. V. Shank, R. Yen, and C. Hirlimann, Phys. Rev. Lett. 50, 454 (1983).
4. D. H. Lowndes, R. F. Wood, and R. D. Westbrook, Appl. Phys. Lett. 43, 258 (1983).
5. M. C. Downer and C. V. Shank, Phys. Rev. Lett. 56, 761 (1986).
6. H. E. Elsayed-Ali, T. B. Norris, M. A. Pessot, and G. A. Mourou, Phys. Rev. Lett. 58, 1212 (1987).
7. P. S. Peercy, in "Laser Surface Treatment of Metals," edited by C. W. Draper and P. Mazzoldi (Martinus Nijhoff, Dordrecht, 1986), p. 611.
8. B. C. Larson, J. Z. Tischler, and D. M. Mills, J. Mater. Res. 1, 144 (1986).
9. D. von der Linde, G. Wartmann, and A. Compaan, Appl. Phys. Lett. 43, 613 (1983).
10. A. Pospieszczyk, M. A. Harith, and B. Stritzker, J. Appl. Phys. 54, 3176 (1983).
11. C. V. Shank, R. Yen, and C. Hirlimann, Phys. Rev. Lett. 51 900 (1983).
12. J. E. Sipe, V. Mizrahi, and G. I. Stegeman, Phys. Rev. B. 35 9091 (1987).
13. J. M. Hicks, L. E. Urbach, E. W. Plummer, and H. Dai, Phys. Rev. Lett. 61 2588 (1988).
14. E. Bauer, Techniques of Metal Research, Vol. II, Part 2, edited by R. F. Bunshah (Interscience, New York, 1969).
15. P. J. Estrup and E. G. McRae, Surf. Science 25, 1 (1971).
16. C. B. Duke and R. L. Park, Physics. Today 25, 23 (1972).

17. D. Lichtman, Methods of Surface Analysis, Vol. I, edited by A. W. Czanderna (Elsevier Sci. Pub., Amsterdam, 1975).

18. A. U. McRae, Science 139. 3553 (1963).

19. M. G. Lagally and J. A. Martin, Rev. Sci. Instrum. 54 1273 (1983).

20. B. A. Joyce, J. H. Neave, P. J. Dobson, and P. K. Larsen, Phys. Rev. B 29, 814 (1984).

21. P. E. Hojlund Nielsen, Surf. Sci. 40, 445 (1973).

22. H. E. Elsayed-Ali and G. A. Mourou, Appl. Phys. Lett. 52, 104 (1988).

23. C. S. Lent and P. I. Cohen, Phys. Rev. B 33, 8329 (1986).

24. G. W. Simmons, D. F. Mitchell, and K. R. Lawless, Surf. Sci. 8, 130 (1967).

25. J. W. M. Frenken, P. M. J. Maree, J. F. van der Veen, Phys. Rev. B 34, 7506 (1986).

26. W. Sibbett, H. Niu, and M. R. Baggs, Rev. Sci. Instrum. 53 758 (1982).

27. K. Kinoshita, M. Ito, and Y. Suzuki, Rev. Sci. Instrum. 58, 932 (1987).

28. I. N. Duling III, T. Norris, T. Sizer II, P. Bado, and G. A. Mourou, J. Opt. Soc. Am. B2, 616 (1985).

29. P. Bado and M. Bouvier, Rev. Sci. Instrum. 56, 1744 (1985).

30. M. J. Eckart, R. L. Hanks, J. D. Kilkenny, R. Pasha, J. D. Wiedwale, and J. D. Hares, Rev. Sci. Instrum. 57, 2046 (1986).

31. B. K. F. Young, R. E. Stewart, J. G. Woodworth, and J. Bailey, Rev. Sci. Instrum. 57, 2724 (1986).

32. J. C. Postlewaite, J. B. Miers, C. C. Reiner, and D. D. Dlott, IEEE J. Quant. Elect. 24, (1988).

33. J. L. Wiza, Nucl. Instrum. Methods 162, 587 (1979).

34. M. H. Van Hove, R. J. Koestner, P. C. Stair, J. P. Biberian, L. Kesmodel, I. Bartos, and G. A. Somorjai, Surf. Sci 3, 189, 218 (1981), and references therein.

35. F. Ercolessi and E. Tosatti, Phys. Rev. Lett. 57, 719 (1986).

36. P. Carnevali, F. Ercolessi, and E. Tosatti, Surf. Sci. 189/190, 645 (1987).

37. P. Carnevali, F. Ercolessi, and E. Tosatti, Phys. Rev. B 36, 6701 (1987).

38. A. R. Ubelohde, The Molten State of Matter (Wiley, New York, 1978).

39. D. P. Woodruff, The Solid-Liquid Interface (Cambridge University Press, London, 1973).

40. D. A. Porter and K. E. Easterling, Phase Transformation in Metals and Alloys (Van Nortrand Reinhold, 1981).

41. R. N. Cahn, Nature 273, 491 (1978).

42. R. A. Lindemann, Z. Phys. 14, 609 (1910).

43. G. S. Zhdanov, Soviet Phys. - Cryst. 21, 706 (1976).

44. A. Pavlovska and D. Nenow, J. Crystal Growth 39, 346 (1977).

45. H. Heyer, F. Nietruch, and I. Stranski, J. Crystal Growth 11, 283 (1971).

46. A. Pavlovska and D. Nenow, Surf. Sci. 27, 211 (1971).

47. K. D. Stock, Surf. Sci. 91, 655 (1980).

48. E. G. McRae and R. A. Malic, Phys. Rev. Lett. 58, 1437 (1987).

49. G. W. Sears, J. Chem. Phys. Solids 2, 37 (1957).

50. M. Volmer and O. Schmidt, Ann. Phys. Chem. 85, 467 (1937).

51. B. Mutaftschiev and J. Zell, Surf. Sci. 12, 317 (1968).

52. W. J. McG. Tegart, "The Electrolytic and Chemical Polishing of Metals in Research and Industry," (Pergamon, New York, 1959).

APPENDIX A

TIME-RESOLVED ELECTRON DIFFRACTION FACILITY
LABORATORY FOR LASER ENERGETICS
UNIVERSITY OF ROCHESTER

The picosecond time-resolved electron diffraction facility at the Laboratory for Laser Energetics (LLE) currently consists of two diffraction systems and supporting equipment. A general view of this facility is shown in Fig. 1. The following is a general brief description of this facility:

(1) The picosecond reflection high-energy electron diffraction (RHEED) shown in Fig. 2 is operated at 10^{-10} Torr. This system consists of two chambers which can be isolated with a 6 in gate value (Fig. 2). This system uses a 300 liter/second ion pump and a titanium sublimation pump to achieve UHV environment in the main chamber. The second chamber is pumped by a 300 liter/second turbomolecular pump supported by a two-stage forepump. The combination of an ion pumped system and turbomolecular pumping allow us a great deal of flexibility in operating pressures. In addition, experiments requiring gas flow are greatly facilitated. A precision manipulator with a heating and cooling stage is used to position the specimen. An argon ion gun and appropriate leak valves are available for the usual surface cleaning operation by sputtering, oxidization, etc. A picosecond photoactivated electron gun (home designed and fabricated) is installed on the main chamber. Electron amplification and detection is performed using microchannel plates and a phosphor screen deposited on a fiber-optics faceplate providing one-to-one imaging of the diffraction pattern.

(2) The transmission picosecond high-energy electron diffraction system (left side of Fig. 2) is operating at a pressure of ~2 x 10^{-6} Torr and uses a liquid nitrogen trapped diffusion pump backed with a roughing pump. This system has been used in all our studies of free-standing thin film heating.

(3) The picosecond regenerative amplifier system (currently time shared with another project) consists of a 100 MHz Nd:YAG ($\lambda = 1.06$ μm) oscillator and a multipass injection-locked amplifier (Fig. 3). This system provides output pulses of ~0.4 mJ/pulse at 1 KHz repetition rate and a pulse width of ~100 ps. This laser system is located in an adjacent room to the diffraction facility shown in Fig. 1. The laser pulses are allowed to pass through the window shown in Fig. 3.

(4) A double-pass amplifier head is used to amplify the output of the regenerative amplifier to 30 mJ/pulse at 8 Hz repetition rate (Fig. 4). Also shown in Fig. 4 is another regenerative amplifier which is currently under construction and which is to be dedicated to the operation of the electron diffraction facility.

(5) The crystal fabrication facility consists of an evaporator with crystal thickness monitor and a heated sample stage (right side of Fig. 5). Thin films (few hundred angstroms) of single crystals and polycrystals of Au and Ag were fabricated in this facility.

(6) A scanning tunneling microscope operating in air (Fig. 6) is used to study laser-induced surface transformation in clean materials. Currently we are examining surface topography of laser melted graphite.